SIMULATION OF STRONG EARTHQUAKE MOTION WITH CONTAINED-EXPLOSIVE LINE SOURCE ARRAYS

Single-Source and Array Tests at Camp Parks

Interim Report
Covering the Period from July 1978 to January 1979

March 1979

By: J. R. Bruce
    H. E. Lindberg
    G. R. Abrahamson

SRI International
333 Ravenswood Avenue
Menlo Park, California 94025
(415) 326-6200
Cable: SRI INTL MNP
TWX: 910-373-1246

50272-101

REPORT DOCUMENTATION PAGE	1. REPORT NO. NSF/RA-790129	2.	3. Recipient's Accession No. PB301096
4. Title and Subtitle Simulation of Strong Earthquake Motion with Contained-Explosive Line Source Arrays, Single-Source and Array Tests at Camp Parks, Interim Report			5. Report Date March, 1979
			6.
7. Author(s) J. R. Bruce, H. E. Lindberg, G. R. Abrahamson			8. Performing Organization Rept. No. SRI Project PYU00993
9. Performing Organization Name and Address SRI International 333 Ravenswood Avenue Menlo Park, California 94025			10. Project/Task/Work Unit No.
			11. Contract(C) or Grant(G) No. (C) (G) PFR7800993
12. Sponsoring Organization Name and Address Engineering and Applied Science (EAS) National Science Foundation 1800 G Street, N.W. Washington, D.C. 20550			13. Type of Report & Period Covered Interim, 7/78-1/79
			14.

15. Supplementary Notes

16. Abstract (Limit: 200 words)

An earthquake simulation technique to aid in the design of earthquake resistant structures is reported. In-situ structures are tested to observe vibration modes and explore potential damage mechanisms in complete soil-structure and internal equipment systems. The technique produces earthquake-like ground motion by simultaneous detonation of a planar array of vertical line sources placed in the soil near the structure to be tested. Both amplitude and frequency are controlled at levels suitable for testing with the source arrays close to the test structure. Tests at one-third scale are described in which single line sources and an array of several sources are implemented. These tests have demonstrated that reasonable amplitudes and frequencies can be coupled into the earth with a minimum of explosive and with no surface eruptions. The tests also show that repeatable results can be obtained with reuse of the same line sources. Plans for testing both single source and multiple source arrays using larger scale models are described. An analytical solution to measure stress, strain, and displacement around a pressurized elliptical hole is given in the appendix.

17. Document Analysis a. Descriptors

Earthquake resistant structures
Earth movements
Underground explosions
Arrays

Shock waves
Scale models
Mathematical analysis

b. Identifiers/Open-Ended Terms
Single source tests
Array tests

c. COSATI Field/Group

18. Availability Statement NTIS	19. Security Class (This Report)	21. No. of Pages 75
	20. Security Class (This Page)	22. Price PC A04/MF A01

(See ANSI-Z39.18)   See Instructions on Reverse

OPTIONAL FORM 272 (4-77)
(Formerly NTIS-35)
Department of Commerce

An earthquake simulation technique to aid in the design of earthquake resistant structures is described. The ten structures are tested to observe vibration modes and on large potential damage reductions in complete soft-sty

SIMULATION OF STRONG EARTHQUAKE MOTION WITH CONTAINED-EXPLOSIVE LINE SOURCE ARRAYS

Single-Source and Array Tests at Camp Parks

Interim Report
Covering the Period from July 1978 to January 1979

March 1979

By: J. R. Bruce
    H. E. Lindberg
    G. R. Abrahamson

Endorsement Co-Principal Investigator	Endorsement Co-Principal Investigator
G. R. ABRAHAMSON	H. E. LINDBERG
[signature]	*[signature]*
Director, Poulter Laboratory	Staff Scientist

INTENTIONALLY BLANK

ABSTRACT

An earthquake simulation technique is being developed to aid in
the design of earthquake-resistant structures. The objective is to
test in-situ structures to observe vibration modes and explore potential
damage mechanisms in complete soil-structure and internal equipment
systems. The technique will be applicable to soil-structre interactions
in general, including those in pipelines, power lines, dams, bridges, and
tunnels.

The technique produces earthquake-like ground motion by simultaneous
detonation of a planar array of vertical line sources placed in the soil
near the structure to be tested. Each line source produces ground motion
through an expandable rubber bladder rugged enough to withstand repeated
tests with expansions as large as twice the initial bladder diameter.
The explosive is detonated inside a steel canister within the bladder,
and the explosion products flow out of the canister through vent holes
to pressurize the bladder at a controlled rate. In this way, both ampli-
tude and frequency are controlled at levels suitable for testing with the
source arrays close to the test structure. This opens the possibility of
in-situ testing at strong shock levels with little disturbance to nearby
structures. In a full-scale test the array might measure 100 ft wide by
35 ft deep, consist of 10 to 20 vertical boreholes 35 ft deep, spaced on
5- to 10-ft centers, and be placed about 25 ft from the structure to be
tested.

To date, tests at 1/3 scale have been performed with single line
sources and also with an array of 10 sources spaced on 3-ft centers. The
rubber bladders were 4 inches outside diameter and 11 ft long, placed
in 15-ft-deep boreholes. In initial tests, single-source accelerations
were 0.5 g at 6 feet, and had dominant frequencies of 15 and 30 Hz. In
the array, lower frequencies were enhanced so that the dominant frequencies

were 8 and 15 Hz, with a peak acceleration of 1 g and a peak velocity of 0.5 fps. In full scale, these translate into about 3 and 5 Hz with a peak acceleration of 0.3 g and a peak velocity of 0.5 fps. This is a useful range for testing and can be extended to lower and higher amplitudes and frequencies by adjusting the amount of explosive and the gas release parameters.

Testing is now under way to demonstrate that multiple detonations can be fired within a single source and to simplify construction and improve the performance of the sources. A large-scale source will be designed and tested later under the current contract. Construction of large-scale arrays for structural testing is planned for next year.

CONTENTS

INTENTIONALLY BLANK

vi

ILLUSTRATIONS

I INTRODUCTION AND SUMMARY

A. Background and Need

The need for an in-situ test technique to aid in the design of earthquake-resistant structures has long been recognized. This need has become more acute with the development of nuclear reactors, greater population concentrations, and the more efficient designs that are made possible by computer technology. During the past two years, SRI International (formerly Stanford Research Institute) has been conducting a program funded by the National Science Foundation to develop an explosive method for testing in-situ structures at strong earthquake levels. The objective of testing in-situ structures is to observe vibration modes and explore potential damage mechanisms in complete soil-structure and internal equipment systems. The technique will be applicable to buildings, nuclear reactors, pipelines, power lines, dams, bridges, and tunnels.

The technique produces earthquake-like ground motion by simultaneous detonation of a planar array of vertical line sources placed in the soil near the test structure. The key feature of each line source is a cylindrical steel canister in which the explosive is detonated. Controlling the release of the high pressure detonation products from this canister allows controlled pressurization of the surrounding soil. In this way, both the amplitude and frequency content are controlled at levels suitable for testing with the array close to the test structure. This opens the possibility of in-situ testing at high levels of earth motion with a minimum amount of explosive and with little disturbance to the surroundings. The duration of the simulated earthquake motion can be controlled by delayed multiple deotnations within each line source and between groups of line sources.

For testing a 30-ft-base structure, the array would probably measure about 100 ft wide and 35 ft deep. It would consist of 10 to 20 line sources placed in vertical bore holes 35 ft deep and spaced on 5- to 10-ft centers, and it would be placed about 25 ft from the structure to be tested. Figure 1 shows one application of the array: testing of a scale model of a nuclear reactor containment building. For a 100 x 35 ft array, the reactor containment building would be approximately 1/5 scale. Other structures of less sizeable dimensions could be tested at full-scale with a similar array. Larger arrays can be built as needed. Results of the current program show that, in general, the array width should be two to three times the plan dimension of the test structure.

During the first year of the program (Grant ENV 76-23273, November 1976 to October 1977) we achieved the following:

- Developed reusable hardware for producing contained explosions in a 1/3-scale line source.

- Incorporated instrumentation for hardware diagnostics and output measurements.

- Demonstrated repeatability of results.

- Obtained reasonable accelerations.

- Obtained reasonable frequencies.

These results are described in detail in an SRI final report[*] and are highlighted in Figure 2. Figures 2(a) through 2(c) show the acceleration measured 5 ft from a single source for three separate tests with the same source. Comparison of these records show the reuseability of the line source and the repeatability of the results. The peak acceleration was 0.8 g with a fundamental frequency of 15 Hz. In full scale, these translate into a 5-Hz frequency with a peak acceleration of 0.3 g.

---

[*] G. R. Abrahamson, H. E. Lindberg, and J. R. Bruce, "Simulation of Strong Earthquake Motion with Explosive Line Source Arrays," SRI Final Report for NSF (October 1977).
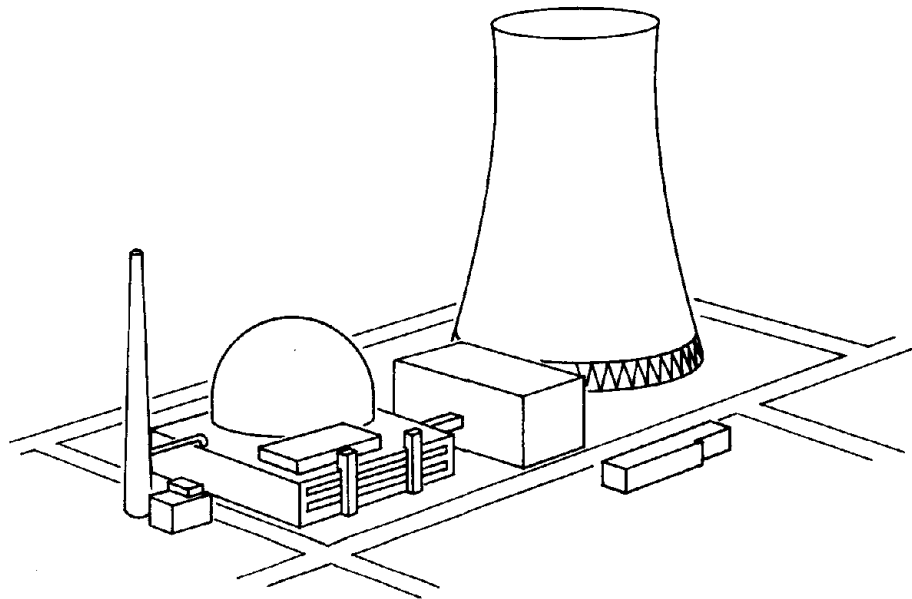
(a) NUCLEAR POWER PLANT
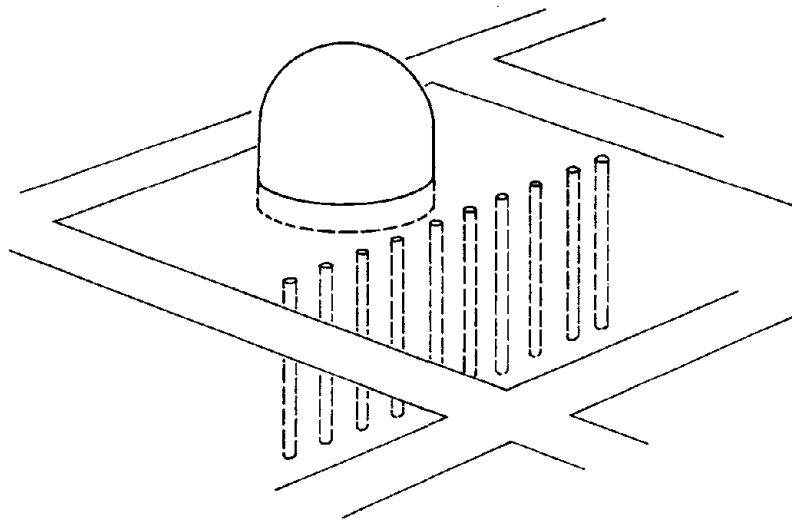
(b) SCALE MODEL TESTING OF CONTAINMENT BUILDING

MA-7556-1A

FIGURE 1   APPLICATION OF ARRAY TO NUCLEAR REACTOR TESTING

3
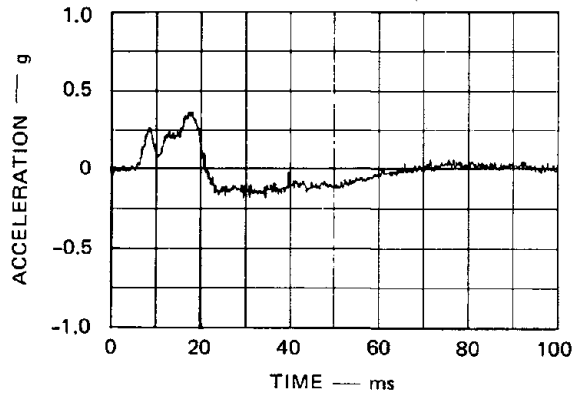
(a) TEST 48, 39 gm PETN, Al

(b) TEST 49, 58 gm PETN, Al

(c) TEST 50, 58 gm, PETN, Al
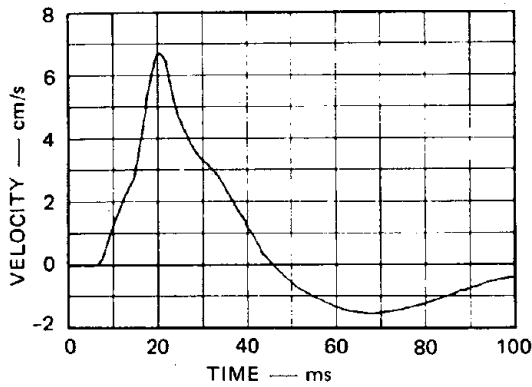
(d) TEST 50, VELOCITY
(INTEGRATED FROM Al)
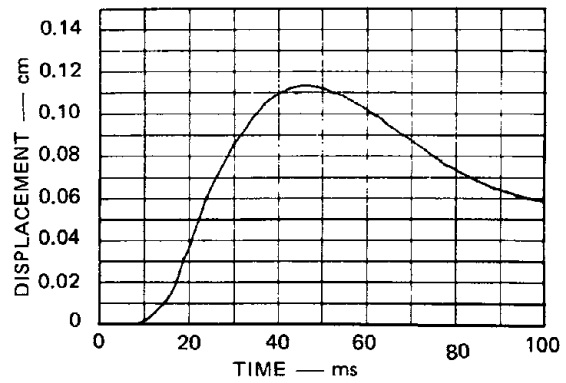
(e) TEST 50, DISPLACEMENT
(INTEGRATED FROM Al)

MP–7556–2

FIGURE 2   SELECTED RESULTS FROM FIRST YEAR OF PROGRAM

Measurements 63 in. from Single Source, 2.0-ft. depth.

4

Figures 2(d) and 2(e) show the velocity- and displacement-time histories from one test; these histories were calculated by integrating the acceleration records.

B.   Current Research Program

The second research program (Grant PFR78-00993, since July 1978) consists of four tasks:
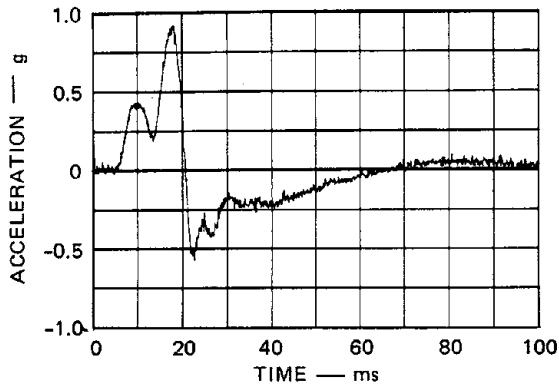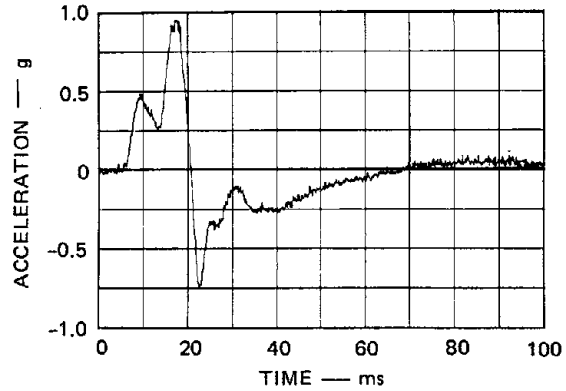
(1) Perform a series of array tests using 10 line sources at 1/3 scale to validate array calculations, and demonstrate energy coupling and ground motion control in array geometry.

(2) Design and test a single large-scale line source to confirm the frequency content, pulse duration, and acceleration levels predicted from the 1/3-scale source measurements.

(3) Perform theoretical analyses of simulation performance, including

–   Interpretation of measured response from single sources and arrays and prediction of earth motion from arrays in other soil types.

–   Investigation of effects of site parameters such as soil type, water saturation, and depth.

(4) Conduct further developmental investigations to

–   Achieve multiple pulses from a single-line source.

–   Vary frequency content.

–   Make design improvements toward a routine field test capability.

–   Improve line source performance, diagnostics, and ground motion instrumentation.

This interim report covers the work performed during the first six months of the above program. During this period we improved the design and performance of the line source developed in the first year's work and performed a series of single-source tests with this improved line source (Task 4), performed a series of array tests using 10 line sources spaced on 3-ft centers (Task 1), and examined theoretically the response of both single sources and arrays (Task 3).

5

During the last half of the current program we will be performing tests to demonstrate that multiple detonations can be fired in a single source and we will be making further modifications to the sources to simplify construction and improve performance (Task 4). We will design and test a large-scale source near the end of the current program (Task 2).

C. Summary of Results

Two series of tests at 1/3 scale were performed at Camp Parks in the Livermore Valley, one series with a single source and the other with an array of 10 sources on 3-ft centers. To allow direct comparison, each series had an identical sequence of explosive charge weights and canister vent areas. The objectives of the experiments were: (1) to compare earth motion from a single source and from an array, (2) to observe the effect on earth motion of nonlinear interaction between sources in the array at plastic soil response levels, (3) to test our ability to control pulse shape and frequency, (4) to compare observed earth motion with motion predicted by simple theory, and (5) to test experimental procedures and source integrity for reuse of the array in several tests.

Results show that soil velocity and displacement for an array test are more than an order of magnitude larger than those at a similar depth and standoff for a single-source test (Figure 23).[*] At a 10-ft standoff from the 1/3-scale array, which contained a total of 2.73 pounds of explosive, the peak velocity was 2.5 in./sec at the mid-depth of the array and 4.2 in./sec near the surface (Figure 20). The peak displacements at depth and at the surface were 0.8 in. and 0.13 in., respectively (Figure 21), and the fundamental period of motion was about 120 msec (8.4-Hz frequency). At full-scale (a 10 x 35 ft array), the corresponding near-surface motions would be at 3 Hz with a peak velocity of 4.2 in./sec and a peak displacement of 0.4 in. The charge weight would be 74 pounds. Because the soil near and between the sources is loaded well into the plastic range, amplitude increases rapidly with charge weight. We

---

[*] See List of Illustrations for locations of figures.

estimate that with 150 pounds of explosive in the 100 x 35 ft array, the velocity and displacement would be increased to about 15 in./sec and 1.5 in., respectively. This is a useful amplitude for structural testing. At this array size, the structure test area is 30 x 30 ft, with a similar test area on the opposite side of the array.

The results also show that the shape and fundamental period of source pressure [Figure 17(a)], and soil stress and displacement (Figure 22) are similar; that is, the fundamental period of the earth motion follows the rise and fall of the source pressure. This is a key observation since it shows that by controlling the source pressure-time history, we can produce earth motion over a wide range of amplitudes and frequencies.

8

II   DESCRIPTION OF EXPERIMENTAL CONFIGURATION

A.   Line Source

A sketch of the line source used for the single source and array tests performed during the reporting period is shown in Figure 3. The source is 1/3 scale of what we envision is required for an array that will shake a 30 x 30 ft test area. The key feature of each line source is a high-strength central steel canister in which the explosive is detonated.[*] The explosive products are then vented at a controlled rate into an expandable rubber bladder rugged enough to withstand repeat tests with expansions as large as twice the initial bladder diameter.

The bladder is 4 in. O.D. with a 0.5 in. wall and is fabricated from 40 durometer pure gum rubber. To keep the bladder from leaking, steel bladder supports are fitted to the top and bottom. A thick rubber sleeve is used to prevent the rubber from tearing at these steel supports. The expandable portion of the rubber bladder was 11 ft. long.

The steel canister has a series of ports into which vent plugs can be fitted. These vent plugs serve two purposes: (1) they redirect the flow from the canister so that it is along the axis of the bladder so that the hot explosive gases do not burn the rubber, and (2) they allow the canister vent area to be readily changed.

This line source has two significant changes from the line source developed during the first year of work. First, a Mylar diaphragm at the top of the source allows the controlled release of the gas from the bladder. This release is accomplished by rupturing the Mylar diaphragm with a small explosive cord, detonated independently from

---

[*]The explosive charge used is Primacord, a convenient and inexpensive form of PETN, produced by the Ensign-Bickford Company, Simsberg, CT.

MYLAR DIAPHRAM

DETONATOR LEAD

2'.5'

15.5'

11.7'

RUBBER SLEEVE

PRESSURE GAGE

EXPLOSIVE CHARGE

RUBBER BLADDER (3 in. I.D. x 4 in. O.D.)

VENT PLUG PORTS

STEEL CANISTER (1.75 in. I.D. x 2.50 in. O.D.)

RUBBER SLEEVE

```
0    4    8    12
└──┴──┴──┴──┘
Scale —— inches
```
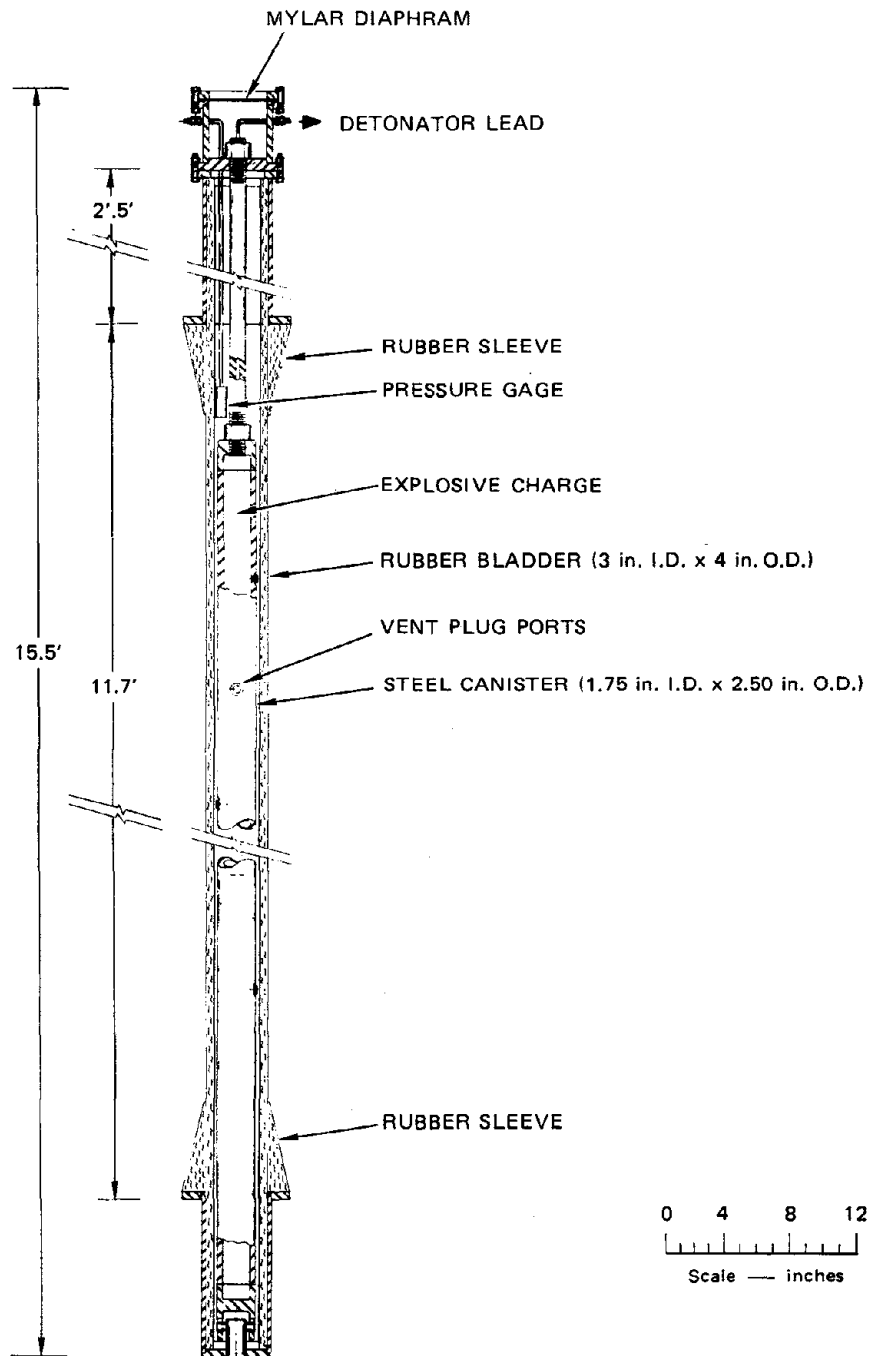
MA-7556-3

FIGURE 3   ASSEMBLY DRAWING OF DEVELOPMENTAL LINE SOURCE

the primary explosive charge. In this way each detonation cycle in the source produces two complete and independently timed oscillations of acceleration. The first results from the initial release of gas from the central canister into the bladder and has acceleration directed away from the source. The second results from the release of gas from the bladder, and has acceleration directed toward the source.

The second change in the line source was introduced to allow us to change the central canister vent area easily without removing the source from the soil. This was accomplished by design of a "turn and lock" connection between the central canister and the bottom cap. This connection allows the central canister to be anchored to the top and bottom caps during a test (providing the necessary axial strength to the line source) while still allowing removal of the canister between tests. To keep the rubber bladder straight and to keep it from collapsing due to the surrounding soil overburden when the central canister is removed, we lined the inside of the rubber bladder with a thin-walled, perforated steel tube.

B. Test Site

SRI maintains a 400-acre remote explosive test site with several instrumentation bunkers near Tracy, California. The first earthquake simulation program was begun there; however, the terrain is hilly and the soil is very rocky, making it a poor test site for the program. At the start of the current program a survey was taken to evaluate alternate sites. A site at Camp Parks, a U.S. Army reserve base near Dublin, CA, was chosen.

A level area within a few hundred feet of power and water was selected for exploration. Previous drilling in nearby areas had indicated the upper 100 to 200 ft of soil to be a fairly uniform deposit of clay. Five 20-ft-deep sampling holes were drilled for our exploration. We obtained soil samples at depths of 3 ft, 10 ft, and 18 ft by driving 3-in.-diameter, 36-in.-long, thin-walled tubes (Shelby Tubes) into the undisturbed soil.

11

The soil stress gage is a design of the U.S. Army Waterways
Experimental Station, Vicksburg, Mississippi, and is currently manu-
factured by Kulite Semiconductor. The design is based on the principle
of a deflecting, rigidly clamped, circular diaphragm. The gage is
wafer-shaped with a sensing diaphragm on both the front and rear surfaces.
Semiconductor strain gages, bonded to the diaphragms, are the sensing
elements. The overall gage assembly is 2 in. in diameter and 0.22 in.
thick.

Figure 4 shows the measurement designation system used for both
the single-source and array tests. The first designation refers to
the type of measurement, the second refers to the sensing direction,
the third refers to either the distance from a single source or the
distance measured perpendicular from the array, the fourth refers to
either an azimuth in degrees for a single source or the distance off
the array centerline, and the last refers to the depth. All distances
are in feet.

A   H   6.0   0.0   7.5

DEPTH FROM SURFACE (Feet), Z

DISTANCE OFF ARRAY CENTERLINE, X
(Azimuth in Degrees for Single Source)

DISTANCE FROM ARRAY, Y
(Source Number for Measurement on Source)

SENSING DIRECTION
H = Horizontal
V = Vertical

TYPE OF MEASUREMENT
P = Bladder Pressure
EX = Bladder Expansion
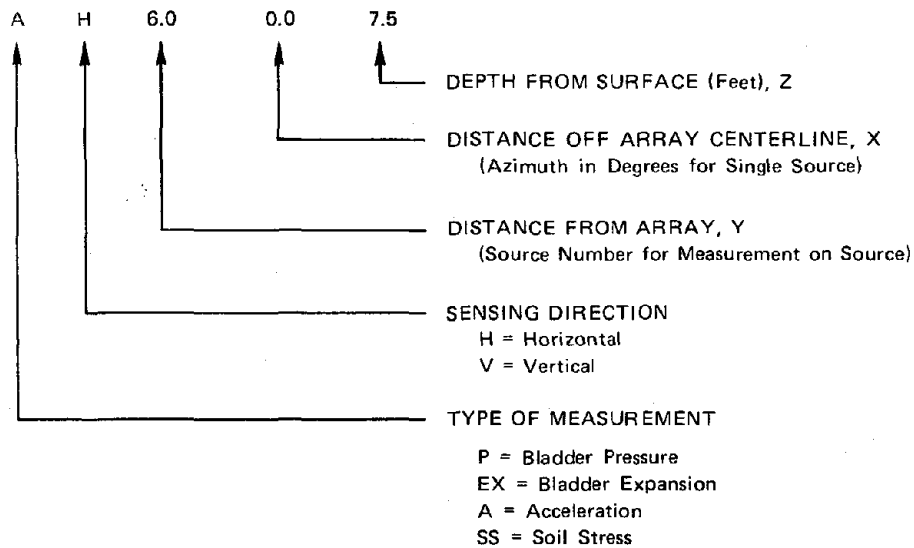A = Acceleration
SS = Soil Stress

MA-7556-6

FIGURE 4   MEASUREMENT DESIGNATION SYSTEM

13

These samples indicated the upper 20 ft of soil to be a fairly uniform deposit of dark grey, stiff clay containing some caliche. The soil samples taken between the 10-ft and 12-ft depth also showed a few randomly oriented lenses of sand 1 to 3 in. thick. The water table was found at 11 ft.

To characterize the soil, the following tests were performed on the soil samples: six unconfined compression tests, a set of consolidated, undrained triaxial tests, and three consolidation tests. The unconfined compressive strength averaged 50 psi at a depth of 3 ft, 25 psi at a depth of 10 ft, and 35 psi at a depth of 18 ft. The water content varied from 60% near the surface to 90% near the water table. The triaxial data showed a friction angle of 30° and a cohesion of 5 to 10 psi.

This area was deemed suitable as the test site. The area was fenced in, an instrumentation trailer was hauled to the site, and power and water lines were run the necessary few hundred feet.

C.   Instrumentation

Four types of instrumentation were used--pressure gages, a bladder expansion gage, accelerometers, and soil stress gages (see Figure 5 in the next section). The pressure gages were used to measure pressure inside the bladder. The bladder expansion gage, developed during the first year, was used to measure the bladder expansion as a function of time. Accelerometers and soil stress gages were placed at various locations in the free field to measure ground motion and stress.

The bladder expansion gage consisted of a 2- x 6- x 0.016-in. steel sheet that was wrapped around the bladder and held in place with a thin rubber sleeve. A strain gage was used to determine the curvature change of the steel sheet and thus the diameter of the rubber bladder. This bladder expansion gage was calibrated in the laboratory and field-checked by comparison with a passive bladder expansion gage consisting of a wire with two slip connections fitted around the bladder. Terminal observation of the wire length gave the maximum bladder expansion during the test for comparison with the active gage.

14

The soil stress gage is a design of the U.S. Army Waterways
Experimental Station, Vicksburg, Mississippi, and is currently manu-
factured by Kulite Semiconductor. The design is based on the principle
of a deflecting, rigidly clamped, circular diaphragm. The gage is
wafer-shaped with a sensing diaphragm on both the front and rear surfaces.
Semiconductor strain gages, bonded to the diaphragms, are the sensing
elements. The overall gage assembly is 2 in. in diameter and 0.22 in.
thick.

Figure 4 shows the measurement designation system used for both
the single-source and array tests. The first designation refers to
the type of measurement, the second refers to the sensing direction,
the third refers to either the distance from a single source or the
distance measured perpendicular from the array, the fourth refers to
either an azimuth in degrees for a single source or the distance off
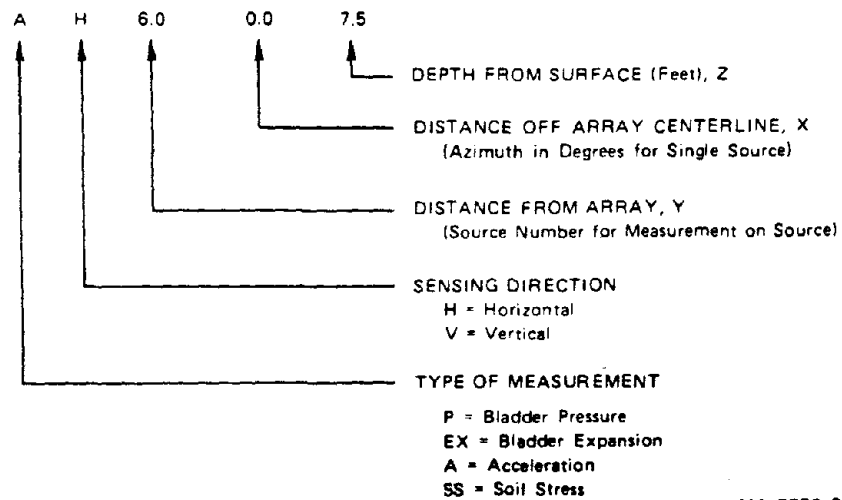the array centerline, and the last refers to the depth. All distances
are in feet.

```
  A      H      6.0      0.0      7.5
  ↑      ↑      ↑        ↑        ↑
  |      |      |        |        └─── DEPTH FROM SURFACE (Feet), Z
  |      |      |        |
  |      |      |        └─────────── DISTANCE OFF ARRAY CENTERLINE, X
  |      |      |                        (Azimuth in Degrees for Single Source)
  |      |      |
  |      |      └──────────────────── DISTANCE FROM ARRAY, Y
  |      |                               (Source Number for Measurement on Source)
  |      |
  |      └─────────────────────────── SENSING DIRECTION
  |                                       H = Horizontal
  |                                       V = Vertical
  |
  └────────────────────────────────── TYPE OF MEASUREMENT

                                         P = Bladder Pressure
                                         EX = Bladder Expansion
                                         A = Acceleration
                                         SS = Soil Stress
                                                                MA-7556-6
```

FIGURE 4   MEASUREMENT DESIGNATION SYSTEM

13

III SINGLE-SOURCE TEST RESULTS

Once the modified line source was designed, the next step was to test a single line source in the soil at Camp Parks. The objectives of these tests were to check the hardware and placement techniques and to obtain data on single-source performance for later comparison to the array performance.

Figure 5 is a schematic of the line source in soil. The source was first placed in a 9-in.-diameter, 15-ft-deep, drilled hole. Figure 6 shows the line source being lowered into the hole. Once the source was in place, the hole was backfilled with a mix containing 73% (by weight) No. 30 sand, 15% clay, 12% water and 0.3%, of CFR2 (a fluidizing agent). The backfilling was accomplished by placing a flexible hose alongside the source and pumping the mix into the hole, filling from the bottom up. The formula for the mix was chosen so that the backfill is relatively incompressible, thus providing good coupling between the source and the surrounding soil, and so that the mix is pumpable, thus greatly simplifying the placement technique with a minimum of voids.

Once the sand/clay mix was pumped to the level of the upper rubber sleeve, the hose was removed and the upper 2.5 ft of the hole was back-filled with saturated sand and tamped. This upper 2.5 ft served as a cap for the semi-fluid sand/clay backfill.

Between tests the upper 2.5 ft of sand was removed, the sand/clay mix was vibrated, and more mix was added, if necessary, to bring the level back up to the upper rubber sleeve. (The amount of mix added varied from a quart to a couple gallons.) The upper 2.5 ft of sand was then replaced and retamped.

In addition to the pressure gages and expansion gages on the source, two accelerometers and a soil stress gage were placed in the surrounding soil. One accelerometer was located at the center-depth of the source (7.5-ft depth) and one was located near the surface (2-ft depth), as

15
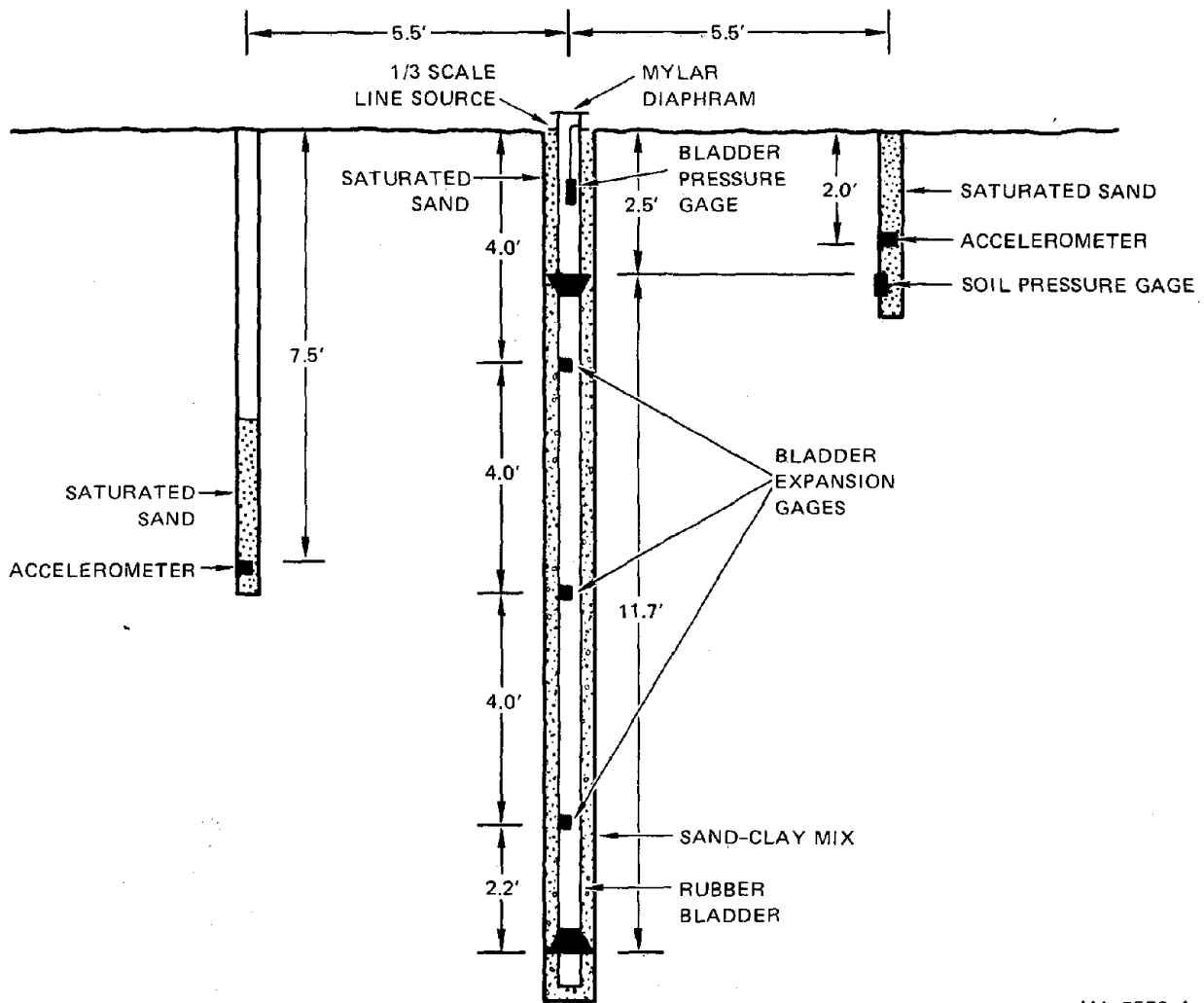
FIGURE 5   SCHEMATIC OF DEVELOPMENTAL LINE SOURCE IN SOIL

MA-7556-4

16
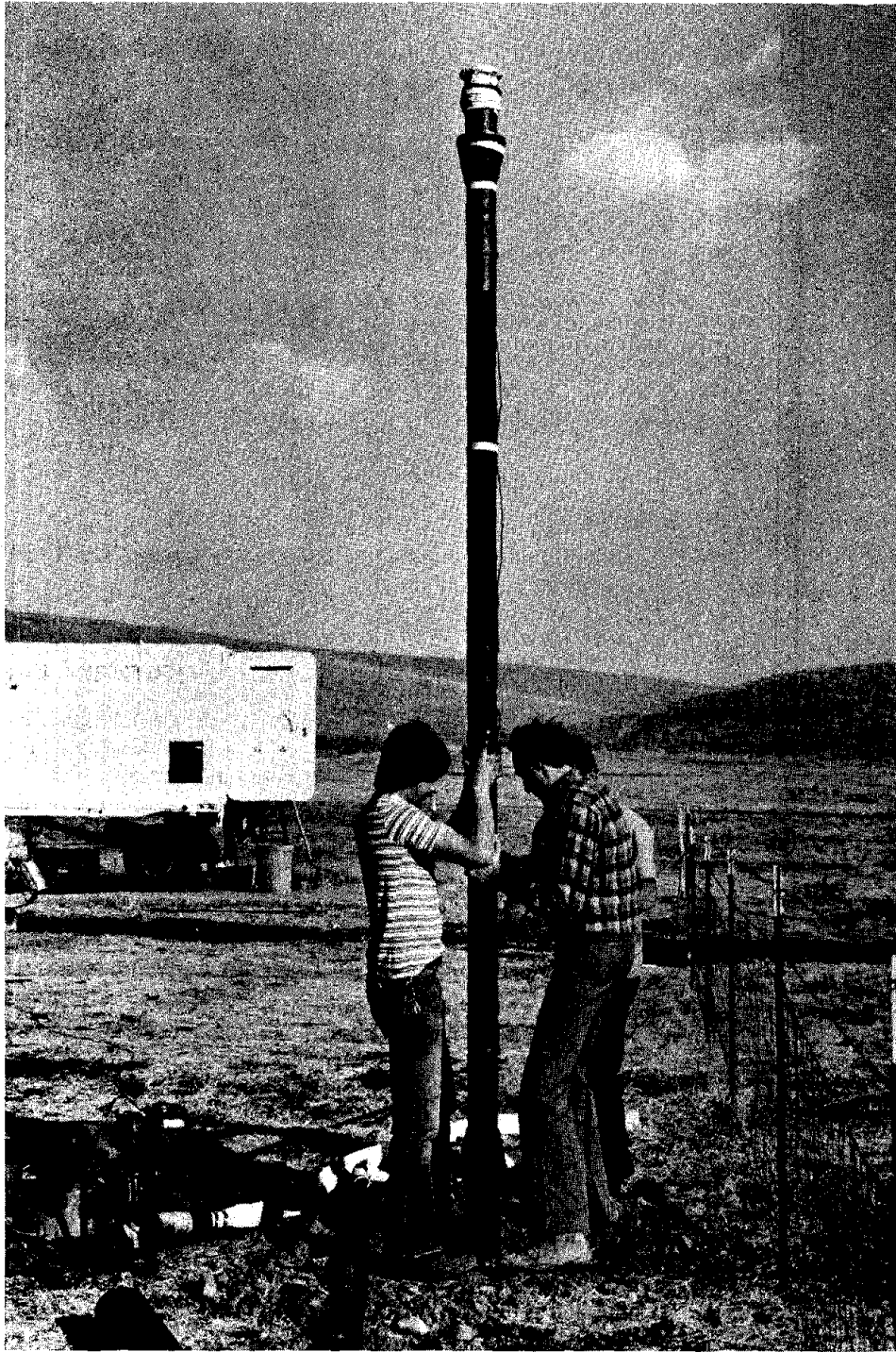
MP-7556-5

FIGURE 6   PLACEMENT OF LINE SOURCE IN SOIL

17

shown in Figure 5. Both accelerometers were oriented with the sensing axis horizontal and with the positive direction radially away from the source. The accelerometers were placed in 6-in.-diameter holes that were backfilled with 2 to 3 ft of saturated sand to ensure good coupling to the soil. The soil stress gage was located at a depth of 2.5 ft in the same borehole as the 2-ft-deep accelerometer. One face of the soil stress gage was pressed into the in-situ soil and then saturated sand was backfilled behind the gage.

For the single-source tests, all free-field measurements were made at a radius of 5.5 ft. This distance was chosen both because it is near a lower bound on the standoff distance for a test structure from an array, and because ground motion amplitude decays quickly with distance from a single source, making it desirable to make measurements close to the source.
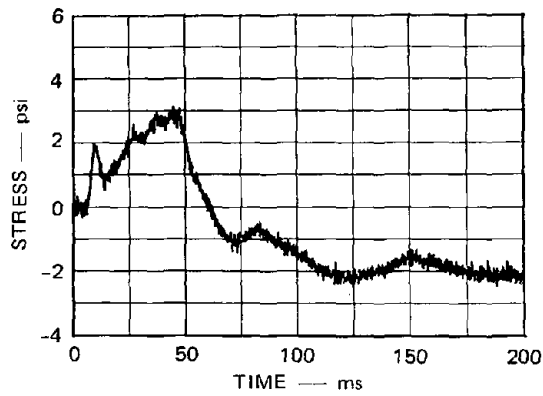
Figure 7 shows the bladder pressure, soil stress, and bladder expansion from a typical single-source test (Test 125) using 10.6 gm/ft of PETN (114 gm total) and a canister vent area of 0.056 in.^{2}/ft. In this test the Mylar exhaust diaphragm was ruptured 40 ms after the primary detonation. The bladder pressure rises almost linearly to near its peak in the first 15 ms and falls suddenly upon rupture of the Mylar diaphragm at t = 40 ms [Figure 6(a)]. This sudden fall in pressure does not represent the true bladder pressure because the gage was located in neck of the bladder 12 in. from the exhaust, and some choking of the flow occurs in this neck. (In later tests this effect was minimized by locating the gage at the base of the neck, 30 in. from the exhaust.)

Comparison of Figure 7(b) with 7(a) shows that soil stress follows the bladder pressure in shape, but has a somewhat slower rise with some ground oscillation superimposed. The soil stress is delayed in time by about 10 ms from the bladder pressure because of propagation time through the soil to the gage.
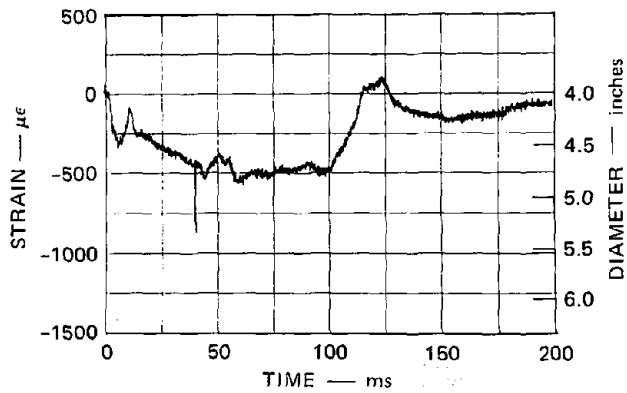
Figure 7(c) shows the bladder expansion record. Importance cannot be placed on the details or the amplitude of the bladder gage response because of the many sources for nonuniform expansion both around the

18
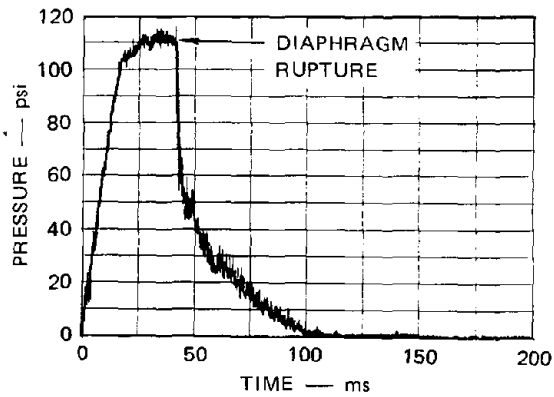
(a) BLADDER PRESSURE

(b) SOIL STRESS 5.5 FEET FROM SOURCE
(AH5.5, 180°, 2.5)

(c) BLADDER EXPANSION
(4 feet deep)

MA-7556-7

FIGURE 7   BLADDER PRESSURE, SOIL STRESS, AND BLADDER
EXPANSION FROM SINGLE-SOURCE TEST
Test 125, 10.6 gm/ft PETN, canister vent area 0.056 in.^{2}/ft.

circumference and along the length of the source. However, the general shape of the bladder expansion record shows that the bladder displacement follows closely the shape of the soil stress during the pressure rise. The return of the bladder to its initial diameter is delayed from the pressure decay because the bladder tends not to collapse until the bladder pressure has dropped to 15 to 20 psi.

Figure 8 shows the earth motion 5.5 ft from a single source for the test discussed above. Figures 8(a) and 8(b) show the acceleration at the 7.5-ft and 2.0-ft depths. The initial high acceleration (3 g) at the 7.5-ft depth [Figure 8(a)] is attributed to the fact that the source pressure has an initial sharp rise and is therefore not well matched to that required for sinusoidal acceleration at the fundamental earth motion frequency. This response interpretation will be discussed later, along with means for reducing these acceleration peaks. The accelerations near the surface [Figure 8(b)] are lower in amplitude and frequency. This is attributed to the stress relief near the surface and the fact that the active length of source doesn't begin until a depth of 3 ft. Water content variation with depth may also play a role in the difference between response at depth and surface.

Figures 8(c) through 8(f) show the velocity and displacement time histories for the two accelerometer locations; these histories were calculated by integrating the acceleration records.* The velocity and displacement at the 7.5-ft depth are very small [Figures 8(c) and 8(e)]. This is consistent with the theory of single-source operation discussed in the next section. The velocity and displacement near the surface are larger than those at depth, which might be attributed to the relief from the free surface [Figures 8(d) and 8(f)]. The acceleration, velocity, and displacement near the surface are also consistent with the results
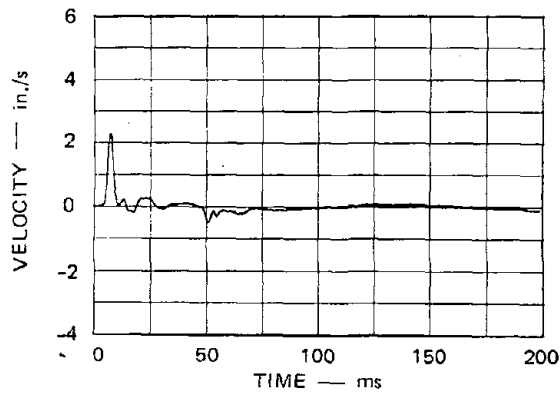
---
*A first-degree polynominal was used to correct the acceleration baseline before integration. The two coefficients were chosen by a standard method, consisting of minimizing the square of the velocity over the duration of the record.
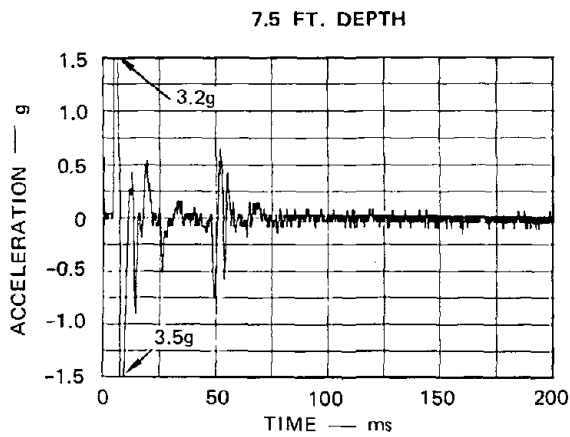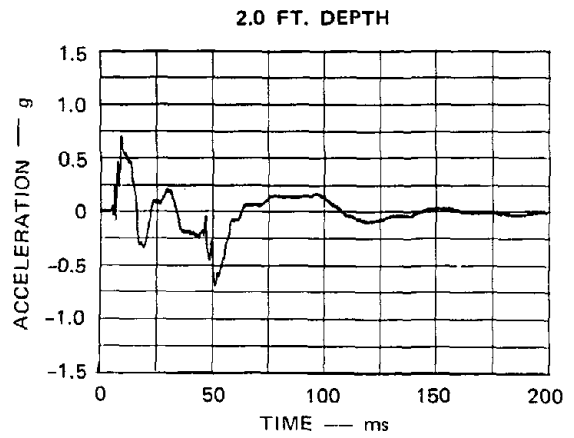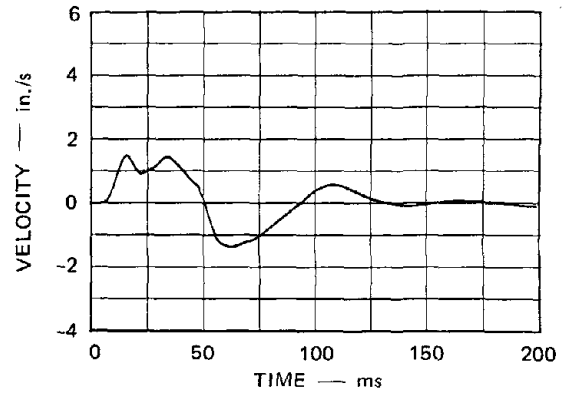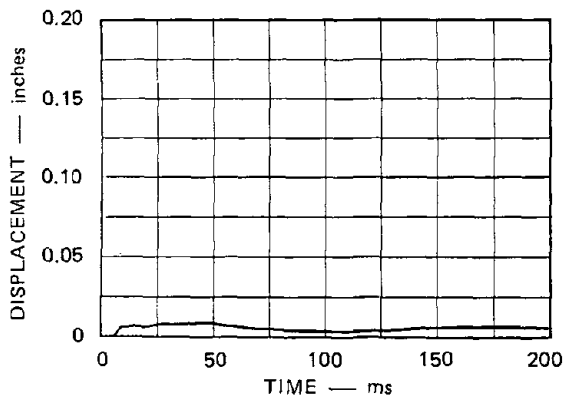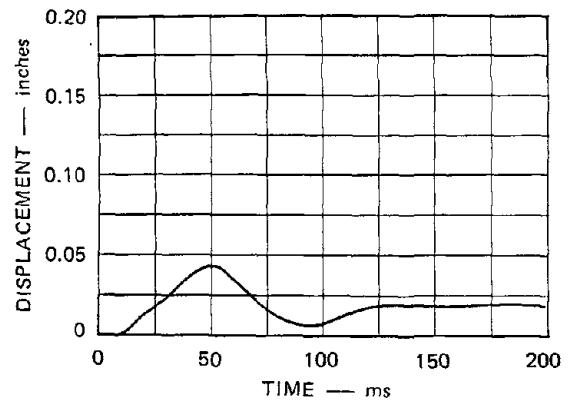
FIGURE 8   EARTH MOTION 5.5 FEET FROM SINGLE SOURCE
Test 125, 10.4 gm/ft PETN, canister vent area 0.056 in.^{2}/ft.

21

of the first year's program, which was performed at a different test site and where acceleration was primarily measured at the 2-ft. depth. (Compare Figure 8 with Figure 2).

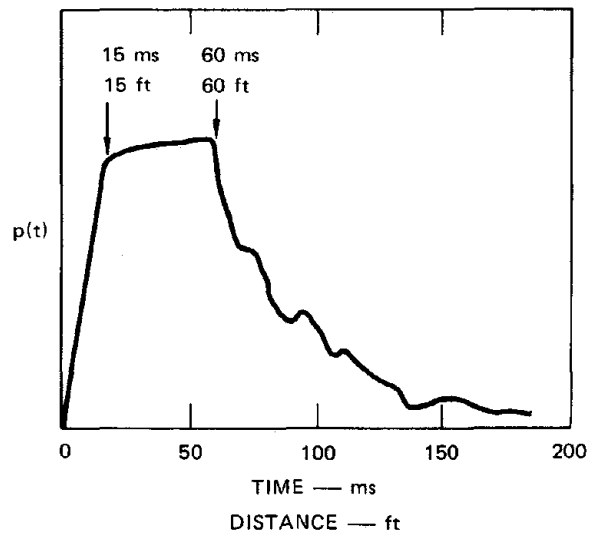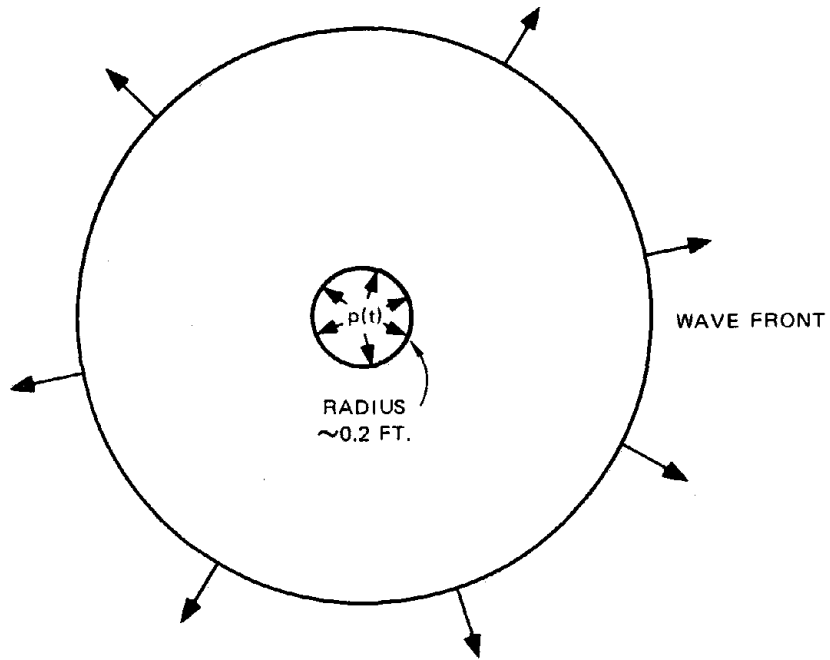## IV   QUASI-STATIC THEORY FOR SINGLE-SOURCE
AND ARRAY RESPONSE

This section describes a quasi-static theroy used to understand the operation of the single source and to extrapolate the single-source results to the array geometry. We present this theory before describing the experimental results for the array because it gives an understanding of the response mechanisms taking place in the array tests and shows clearly the reason for testing with an array.

The basis of the quasi-static theory is shown in Figure 9. The wave front moves about 15 ft (75 source radii) during the pressure rise, indicating that a static theory can be used for displacement near the source. During the duration of the complete pulse, the wave front has moved about 100 ft; therefore, a static theory can be used for overall estimates of displacement from a single source at ranges of interest for structural testing (5 to 15 ft for this source). For the array, these wave front propagation distances are comparable to the 30 x 15 ft array dimensions (a 1/3-scale array), but a static theory is still useful to interpret some features of response and to show the relationship between array and single-source response. Use of a static theory can also be justified by the experimental observation made in the next section that displacement follows the source pressure, the basic characteristic of quasi-static response.

A.   Single Source

To estimate the elastic response around a single source, we consider the static plane strain problem of a pressurized circular hole with radius a_s. The displacement u at a distance r for this idealization would be

$$u = \frac{P(1 + \nu)}{E} \frac{a_s^2}{r}$$

(1)

23

RADIUS
~0.2 FT.

WAVE FRONT

15 ms 60 ms
15 ft 60 ft

p(t)

0   50   100   150   200

TIME — ms

DISTANCE — ft

MA-7556-9

FIGURE 9   COMPARISON OF SOURCE DIMENSIONS
WITH WAVE FRONT LOCATION

24

in which E is Young's modulus, ν is Poisson's ratio, and P is the source pressure. The source pressure is defined as the pressure of the bladder on the surrounding soil and is approximately 20 psi less than the bladder pressure at expansions greater than 25%. (The 20-psi pressure is carried by the hoop stress in the rubber.)

For values of E, ν, and P consistent with the single-source test described in Section III (E = 5000 psi, ν = 0.25, P = 75 psi)

$$u = \frac{75(1 + 0.25)}{5000} \frac{a_s^2}{r} = 0.019 \frac{a_s^2}{r} \tag{2}$$

At a radius of 5.5 ft with a_s = 0.2 ft, we have u = 0.0016 in. Thus, displacements for entirely elastic response would be extremely small because the source dimension a_s is so small compared with the standoff r.

However, near the source the soil yields[*] when the source pressure increases above an initial yield pressure P_y. As P is increased further, a plastic zone of increasing radius R is formed as indicated in Figure 10. If the soil is treated as a Mohr-Coulomb material with unconfined strength σ_u and friction angle ϕ, the initial yield pressure is given by

$$P_y = \frac{\sigma_u}{N_\phi + 1} \quad , \quad \text{where} \quad N_\phi = \frac{1 + \sin\phi}{1 - \sin\phi} \tag{3}$$

As the source pressure increases, the radial stress σ_r at the boundary r = R remains at this yield value P_y, but R increases. The elastic solution for r $\geq$ R has the same form as already given, so that the displacements are now given by

$$u = \frac{P_y(1 + \nu)}{E} \cdot \frac{R^2}{r} \qquad\qquad P \geq P_y \tag{4}$$

---

[*]The soil also compacts immediately around the source, but this affects mainly the deformation at the source hole and hence the gas energy required to maintain the pressure P. In the present analysis, P is taken as a known quantity from the experiments. A theory with more complete soil constitutive relations is planned for future work.
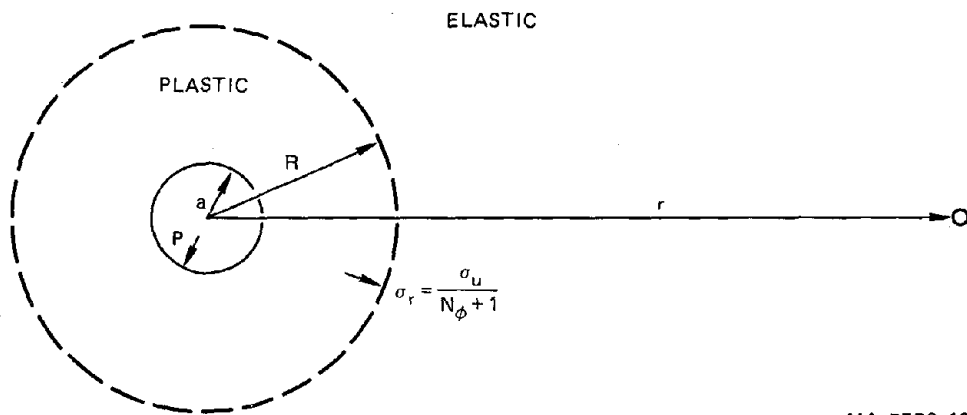
FIGURE 10   SINGLE-SOURCE ELASTIC-PLASTIC MODEL

MA-7556-10

in which

$$\frac{R}{a_s} = \left\{ \frac{N_\phi + 1}{2N_\phi} \left[1 + (N_\phi - 1) \frac{P}{\sigma_u} \right] \right\}^{\frac{N_\phi}{N_\phi - 1}}$$
(5)

For typical soils and, in particular, from measurements made on the soil at the Camp Parks test site, $\phi = 30°$ and the plastic radius and yield pressure are given by

$$\frac{R}{a_s} = \left(\frac{1 + 2P/\sigma_u}{1.5} \right)^{1.5} \qquad P_y = \frac{\sigma_u}{4}$$
(6)

It is useful to also express the postyield displacement in Eq. (4) as a multiple of the displacement u_y at initial yield $P = P_y$, which is given by Eq. (4) with $R = a_s$. Then Eq. (4) becomes simply

$$\frac{u}{u_y} = \left(\frac{R}{a_s} \right)^2$$
(7)

in which

$$u_y = \frac{\sigma_u (1 + \nu)}{(N_\phi + 1)E} \frac{a_s^2}{r}$$
(8)

These results are displayed graphically in Figure 11 for $\phi = 30°$. As P/σ_u increases from 0.25 at initial yield to $P/\sigma_u = 2.5$, the yield radius grows from $R/a_s = 1$ to $R/a_s = 8.0$. The displacement increases from $u/u_y = 1$ to $u/u_y = 64$. If the soil were to remain elastic over this pressure increase, the displacement would increase linearly to $u/u_y = 10$, as shown by the straight line drawn through the initial yield point. The plastic deformation therefore increases the displacement 6.4 times

27
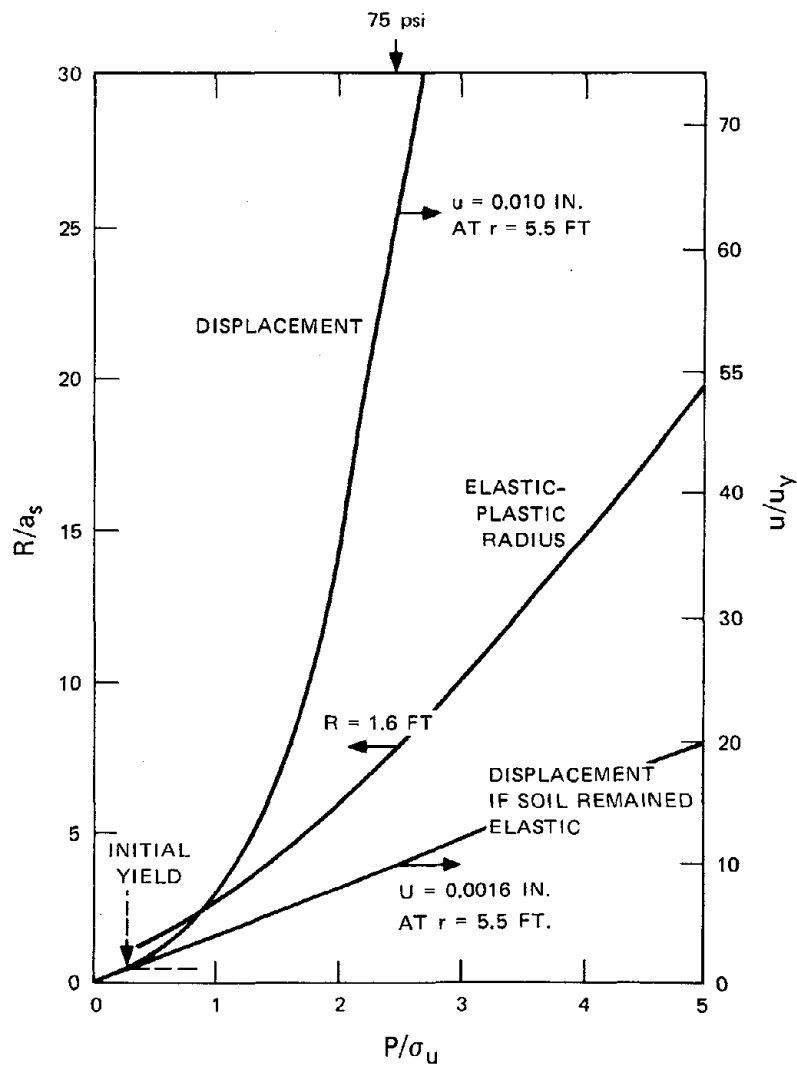
MA-7556-11

FIGURE 11 SINGLE-SOURCE DISPLACEMENT AND ELASTIC-PLASTIC
RADIUS VERSUS PRESSURE

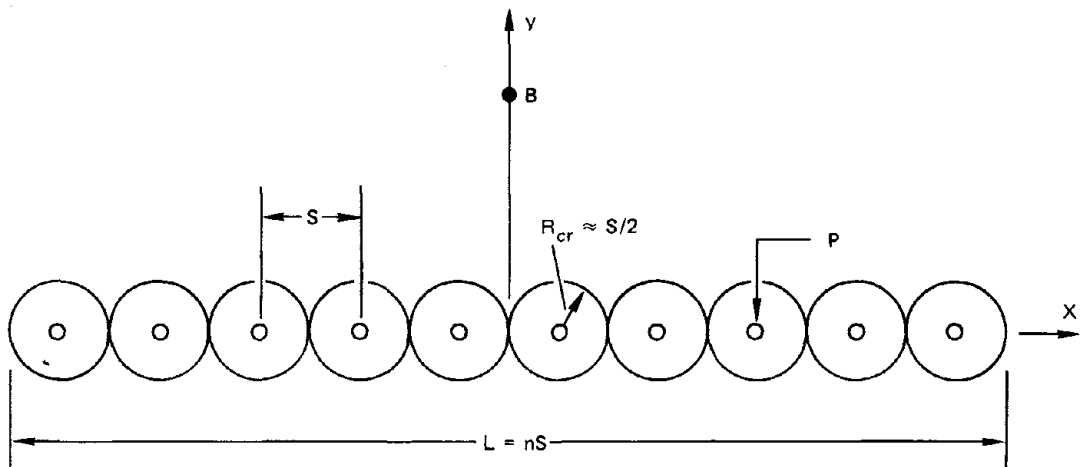Numerical values for soil and source configuration at Camp Parks.

28

that in an entirely elastic deformation. This factor increases sharply as P increases still further. At $P/\sigma_u = 4$, the displacement for plastic deformation is 35.4 times that for a hypothetical elastic deformation.

Tests on soil samples from Camp Parks gave an unconfined compressive strength near 30 psi. Thus, the soil would have yielded at P = 30/4 = 7.5 psi. The displacement 5.5 feet from the single source (the accelerometer location in the single-source tests) for P = 7.5 psi, is u_y = 0.00016 in., found from Eq. (8). The displacement at the example pressure of P = 75 psi, from Eq. (7), is $u = u_y(8)^2$ = 0.010 in. This is still a very small displacement.

From a practical standpoint, the displacement from a single source will always be small. With properties measured for the Camp Parks soil, which are typical of many soils, the displacement given by Eq. (4) at radius r is $u = 0.002R^2/r$, where R is the radius of the elastic-plastic boundary. If we are to have elastic-free-field response at the test structure location we must have R < r. Thus, u < 0.002 r.

B. Array

From the displacement expression given by Eq. (4), we conclude that to increase the displacement in the structural test area, the characteristic dimension of the elastic boundary at which loading is applied must be increased. An array of sources accomplishes this objective while also keeping the source pressure and plastic region reasonably small. This is shown schematically in Figure 12. Pressure is applied in each source until the plastic radius R around each source interacts with the adjacent sources. The result is an overall elastic-plastic interface for the array that is approximately elliptical, with minor diameter s and major diameter ns, where n is the number of sources at spacing s. For simplicity, the individual plastic boundaries around the sources are drawn circular, neglecting the interaction between sources. To estimate quantitative results, we further assume that the elliptical approximation is valid when these circles make first contact, at R = s/2 as shown in Figure 12.

FIGURE 12   ARRAY GEOMETRY

Appendix A gives a complete description of elastic stresses and displacements in the field around an elliptical hole under pressure P_e. The central displacement perpendicular to the array at a distance $y = 0.34$ ns (shown by point B in Figure 12, and corresponding to a 10-ft standoff for the 30-ft array in the tests) is

$$u = \frac{P_e(1 + \nu)}{E} \ (a + b) \tag{9}$$

where a and b are the major and minor radii of the ellipse. In our idealization, $a + b = (ns + s)/2$. Comparison of Eq. (9) with Eq. (4) shows that in going from a single source to an array the characteristic length multiplying either $P_y(1 + \nu)/E$ or $P_e(1 + \nu)/E$ has been increased from R^2/r to $a + b$. With $R = s/2$ and standoff $r = y = 0.34$ ns (10 ft for the array tested, the length ratio is

$$\frac{(a + b) \ r}{R^2} = \frac{\frac{1}{2}(ns + s)(0.34 \ ns)}{(s/2)^2} = 0.68 \ (n^2 + n) \tag{10}$$

For the ten-source array in the tests (n = 10), this ratio is 75.

As a first estimate of the pressure P_e on the elastic boundary of the ellipse, one can ignore the interaction of the sources. This pressure then becomes the same as the pressure P_y acting on the elastic boundary of each single source, that is, 7.5 psi for the soil at Camp Parks. With P_e equal to P_y, the length ratio given by Eq. (10) becomes equal to the ratio between a single source and an array displacement, thus predicting an increase of 75-fold in displacements for the array as compared with a single source. (Note also that the increase is an order of magnitude larger than that from a linear superposition of 10 sources.)

The calculated displacement using $P_e = P_y = 7.5$ psi is 0.36 in. for a 10-ft standoff from an array. A similar calculation at a 6-ft standoff gives a displacement of 0.40 in. The source pressure corresponding to $R = s/2$ (where each elastic single-source boundary moves out to reach

31

the hypothetical boundary of the ellipse) and therefore to these displacements, is 75 psi (Figure 11).

C.   Limitation of the Theory and Future Code Calculations

Array tests with a source pressure of 75 psi (described in Section V) gave measured displacements at the 7.5-ft depth of 0.09 in. at a standoff of 6 ft and 0.08 in. at a standoff of 10 ft. These values are a factor of 4 smaller than those calculated above. The primary reasons for the difference are:

(1)   The theory neglects the complex plastic interaction
       between sources. The preceding calculation gives only
       a rough estimate of displacement and then only for
       displacement at incipient formation of the elastic-
       plastic boundary around the array. For example, soil
       stress measurements in the array tests described in
       Section V, gave σ = 4 psi near the boundary with a
       source pressure of 75 psi, about half that in the
       calculation.

(2)   The quasi-static theory neglects the dynamic response,
       and thus introduces some error at the scale of the
       complete array.

(3)   The plane strain theory neglects the presence of the
       soil free surface and the finite depth of the array.

Nevertheless, the theory gives a reasonable picture of the response mechanisms taking place, and of the relationships between a single source and an array. It also shows how the source and soil parameters affect response and hence gives a guide to use for improvements of explosive arrays.

More complete theoretical analyses that treat all of these short-comings, both individually and in appropriate groups as theoretical complexity is increased, are being performed with a finite element elastic-plastic code. A code calculation is being performed to show the relationship between the source pressure and the pressure on the elliptical boundary, with the complex plastic interaction of the sources taken into account. A preliminary finite element grid is shown in Figure 13(a).

32
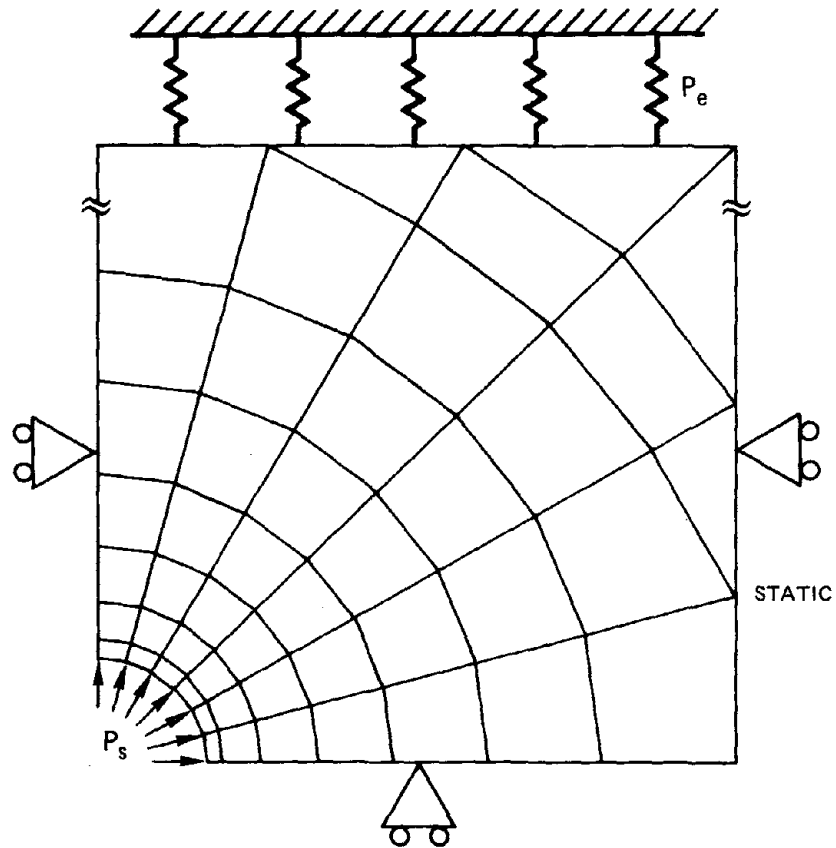
(a) CODE CALCULATION SHOWING RELATION
BETWEEN SOURCE PRESSURE AND PRESSURE
ON ELLIPTICAL BOUNDARY
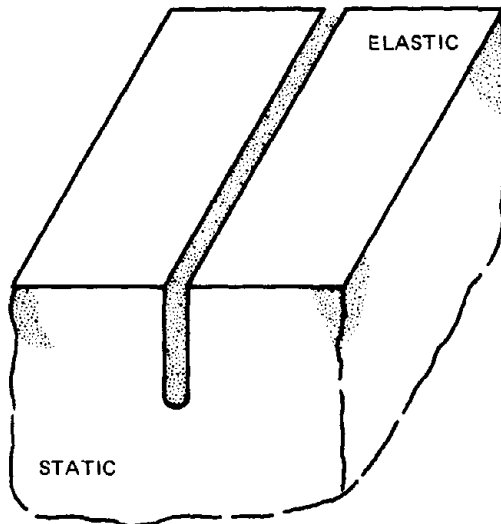
(b) INFINITE SURFACE CRACK IN
ELASTIC HALF-SPACE
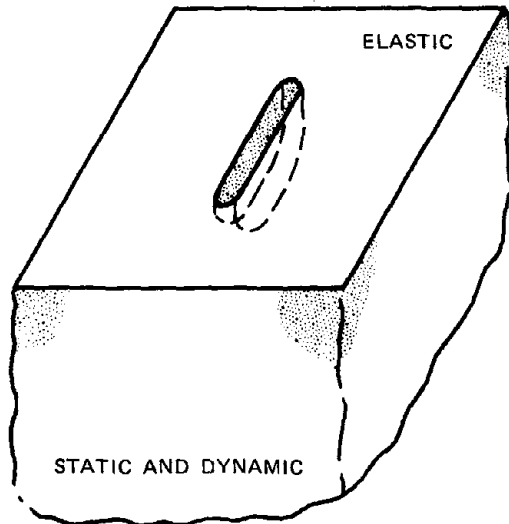
(c) FINITE SURFACE CRACK IN
ELASTIC HALF-SPACE

MA-7556-22

FIGURE 13 THEORETICAL EFFORT FOR REMAINDER OF THIS YEAR'S PROGRAM

33

An individual source in an array is modeled. Symmetry boundaries are placed along the lines of symmetry of the source and along the line symmetry between two sources. The elliptical boundary is represented by a series of elastic springs. The spring stiffness is determined from the pressure/displacement relation for the pressurized elliptical hole. In this manner the finite length of the array is taken into account. A Mohr-Coulomb, elastic-perfectly plastic material model is being used to represent the soil.

The solution for an infinite surface crack in an elastic half-space is being examined to determine the effect of the soil free surface and the finite depth of the source [Figure 13(b)]. This solution exists in the literature for the static case.

Finally, the solution for a finite surface crack in an elastic half-space will be examined [Figure 13(c)]. This solution also exists in the literature; however, the computations are quire lengthy. For this reason we will probably use a finite element code to determine the solution. The code will be run both statically and dynamically to determine the effect of the dynamic response of the soil on the displacement.

V   ARRAY TEST RESULTS

A.   Test Description

Figure 14 shows the array layout. Ten sources were spaced on 3-ft
centers. The sources and the source placement technique were the same
as that for the single-source test described in Section III. The
measurement designation system is given in Figure 4. Bladder pressure
and bladder expansion were measured for two of the ten sources, one
near the center and one at the outer edge of the array. At the 7.5-ft
depth, three accelerometers were located along the array centerline at
standoff distances of 6, 10, and 15 ft, and two accelerometers were
placed 6 ft to the left and 6 ft to the right of the array centerline at
a 6-ft standoff. Accelerometer coverage at the 2-ft depth consisted of
two accelerometers located near the array centerline, one at a 6-ft stand-
off and one at a 10-ft standoff (near the center of the useful test area).
All seven of the accelerometers mentioned above were oriented with their
sensing axis horizontal and perpendicular to the array, with the positive
direction away from the array. A single vertically oriented accelerometer
was located at a standoff of 10 ft and a depth of 1 ft. The sensing
direction was oriented with the positive direction upward.

Soil stress was measured both at a 3-ft standoff (near the equiva-
lent elliptical boundary) and at a 10-ft standoff (where a test structure
would be located). The sensing direction was horizontal and perpendicular
to the array and the depth was 2.5 ft for both gages.

Figure 15 shows a closeup of three of the ten sources in the array.
The Mylar diaphragm used to seal the exhaust vent can be seen. This view
is before hookup of the detonation system.

Figure 16 shows a view of the complete array after hookup of the
detonation system. A steel I-beam was placed behind the row of charges
to shield the sources from a small strand of explosive cord that was
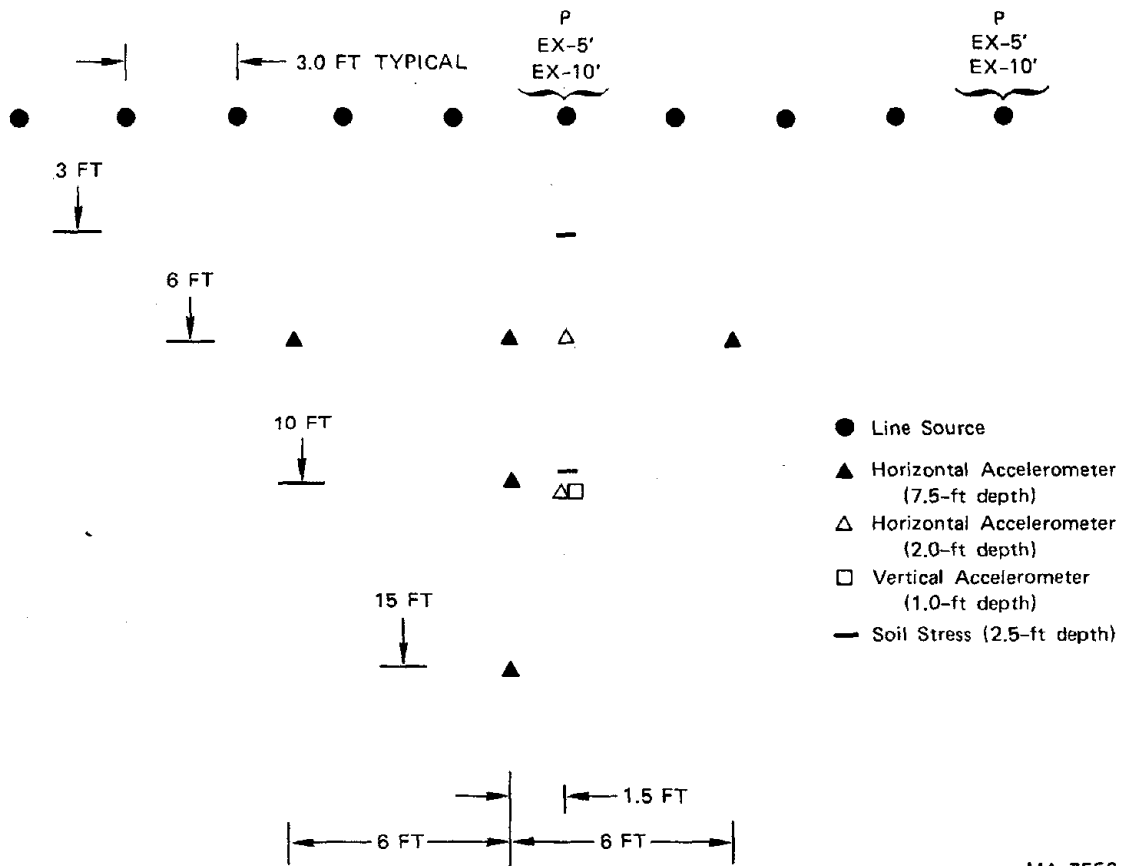
FIGURE 14 ARRAY LAYOUT (PLAN VIEW)

MA-7556-13

MP-7556-29

FIGURE 15   CLOSE-UP OF THREE SOURCES IN ARRAY

(Before hook-up of detonation system)

MP-7556-14

FIGURE 16   VIEW OF LINE SOURCE ARRAY

used to initiate the primary charge in each source. This cord was in turn initiated with a detonator at the center of the array. Since the detonation rate in the cord is 22 ft/ms, the central sources were detonated 0.6 ms ahead of those at the ends of the array (giving, in effect, a simultaneous detonation when compared to the time for the 150-ms complete pulse.)

A second small, continuous, explosive cord was tied to each Mylar diaphragm. This cord was also detonated at its center, rupturing each Mylar diaphragm at a preselected time after the primary detonation. This delay time was either 60 or 100 ms, depending on the test.

Four array tests were performed. Three tests were performed with the same charge size (10.6 gm/ft) but with varying canister vent areas (Test 131, 0.014 in.^{2}/ft; Test 130, 0.028 in.^{2}/ft; and Test 132, 0.056 in.^{2}/ft). One test was performed with a smaller charge size and the median canister vent area (Test 127, 7.0 gm/ft, 0.028 in.^{2}/ft).

B.   Results of Typical Test

Figure 17 shows the bladder pressure, soil stress, and bladder expansion from the array test (Test 132) with 10.6 gm/ft of PETN (114 gm per source) and a canister vent area of 0.056 in.^{2}/ft (the largest vent area tested). In this test the Mylar exhaust diaphragms were ruptured 60 ms after the primary detonation. The records in Figure 17 for an array are similar to those in Figure 7 for a single source, indicating that there is little difference in source pressure and soil stress between single source and an array. (The Mylar diaphragm was ruptured at t = 40 ms for the single source and at 60 ms for the array.) As discussed below, there are differences in the ground motion for the two tests.
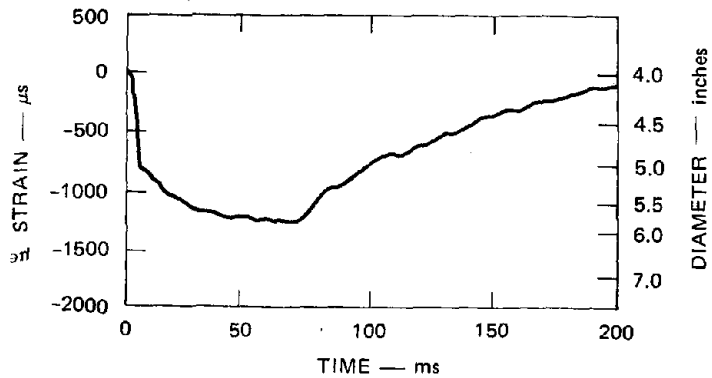
Comparison of Figure 17(b) with 17(a) shows that the soil stress follows the bladder pressure in shape, but has a somewhat slower rise. This result is similar to that for the single-source test (Figure 7). Comparison of 17(c) with 17(a) shows that the bladder expansion also follows the bladder pressure.
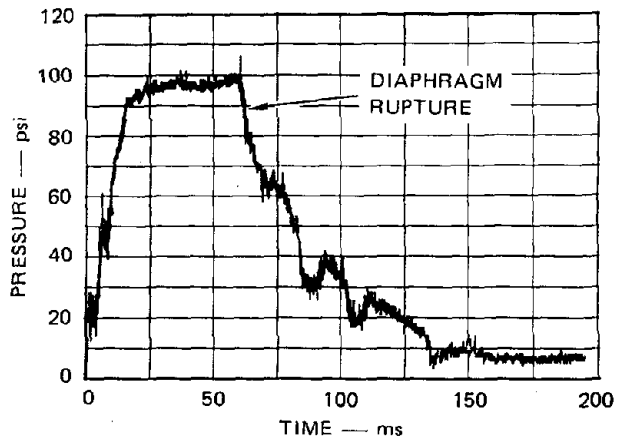
(a) BLADDER PRESSURE (Source 6)
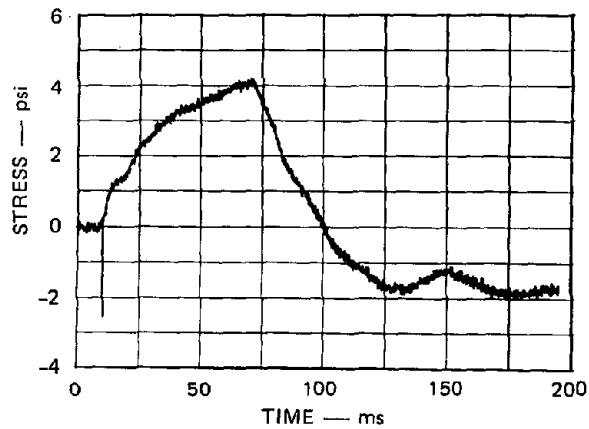
(b) SOIL STRESS 10 FEET FROM
ARRAY (SP10, 1.5, 2.5)

(c) BLADDER EXPANSION
(Source 6, 10 ft. depth)

MA-7556-15

FIGURE 17   BLADDER PRESSURE, SOIL STRESS, AND
BLADDER EXPANSION IN ARRAY TEST

Test 132, 10.6 gm/ft PETN and canister vent
area 0.056 in.^{2}/ft per source.

40

Figures 18(a) and (b) show two symmetric acceleration measurements for Test 132, one made 6 ft to the left and the other 6 ft to the right of the array centerline at the 7.5-ft depth. The motion is essentially the same at the left and right location, demonstrating the uniformity of the soil and of the source response. Comparison with records in Figures 19, 20, and 21 from the central accelerometer shows that soil response is also uniform along the 12-foot span of the accelerometer array. Just as in the single-source tests, the initial accelerations are very high (6 g). This is again attributed to the initial sharp rise in source pressure. This rise will be reduced in future tests to more closely match the shape required for sinusoidal acceleration.

Figures 18(c) through 18(f) show the velocity- and displacement-time histories for the two symmetric accelerometer locations. In contrast to the single-source results (see Figure 8), the velocity and displacements are now appreciable.

Figure 19 shows the six accelerometer records from the array center-line for the same test (Test 132). Figures 19(a), 19(c), and 19(e), from the 7.5-ft depth, again show very high initial acceleration and frequency. These high accelerations attenuate quickly with distance [compare Figure 19(a) with 19(e)].

Figures 19(b) and 19(d) show the records from near the surface (2-ft depth). As in the single-source tests, these accelerations are lower in amplitude and frequency than those at depth, a result attributed to stress relief near the surface and the fact that the active source length begins at a depth of 3 ft.

Figure 19(f) shows significant vertical acceleration at a 10-ft standoff and a 1-ft depth. However, Figure 21(f) shows that there is very little vertical displacement associated with this acceleration.
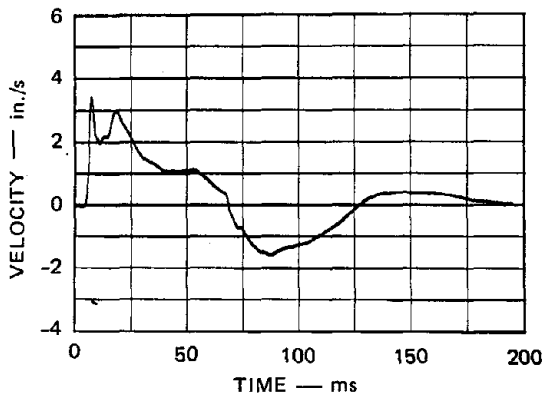
Figure 20 shows the velocity-time histories calculated by integrating the six accelerometer records given in Figure 19. In contrast to the single-source results (see Figure 8), the velocities are significant both at depth and near the surface.
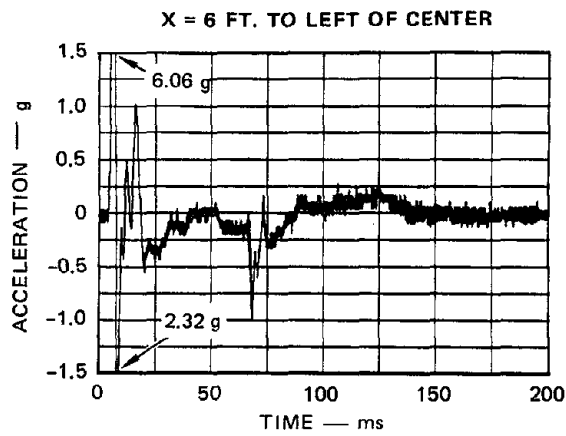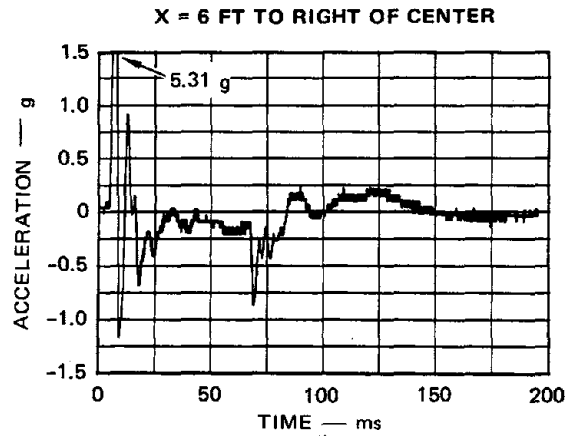
41
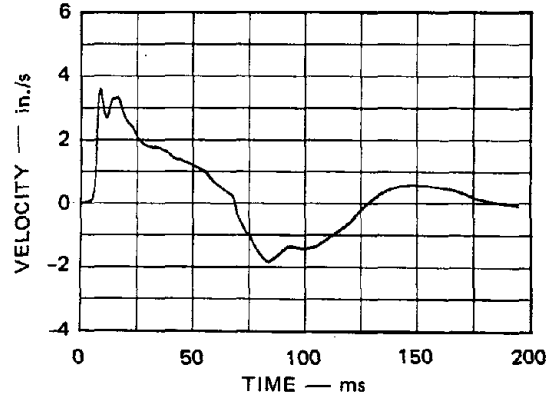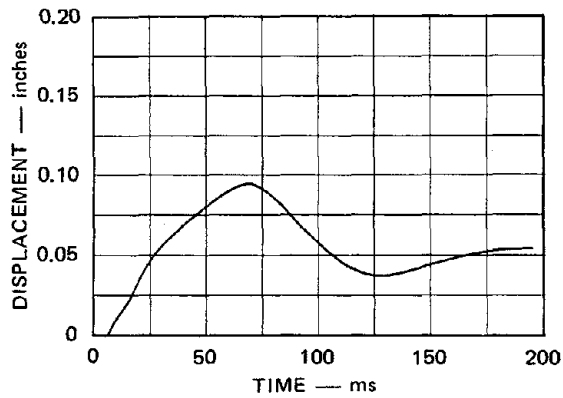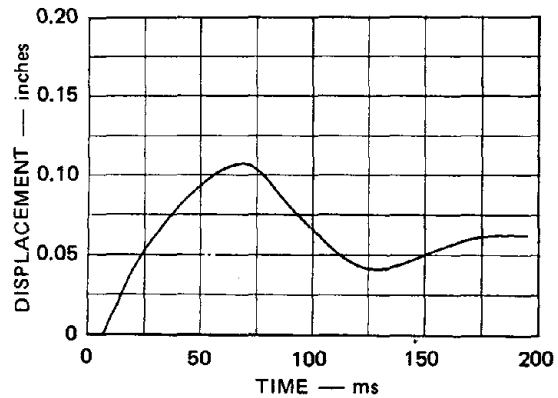
FIGURE 18   EARTH MOTION FROM ARRAY TEST, AT Y = 6 FEET FROM ARRAY AND
Z = 7.5 FEET DEEP

Test 132, 10.6 gm/ft PETN and canister vent area 0.055 in.^{2}/ft per source.

42
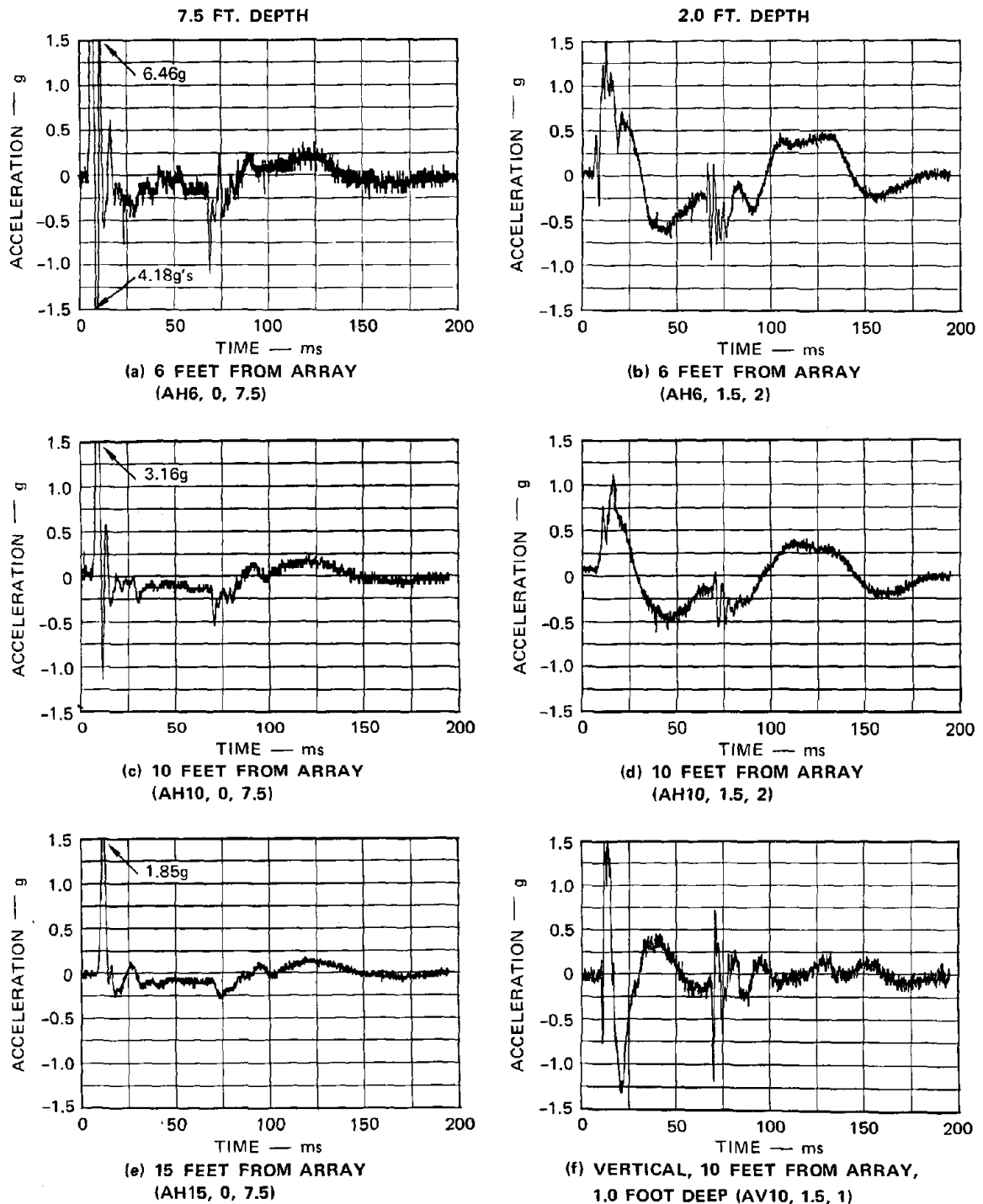
FIGURE 19   VARIATION OF ACCELERATION WITH DISTANCE AND DEPTH FOR ARRAY TEST

Test 132, 10.6 gm/ft PETN and canister vent area 0.055 in.^{2}/ft per source.

43

7.5 FT. DEPTH

(a) 6 FT FROM ARRAY
(AH6, 0, 7.5)

(c) 10 FEET FROM ARRAY
(AH10, 0, 7.5)

(e) 15 FEET FROM ARRAY
(AH5, 0, 7.5)

2.0 FT. DEPTH

(b) 6 FEET FROM ARRAY
(AH6, 1.5, 2)

(d) 10 FEET FROM ARRAY
(AH10, 1.5, 2)

(f) VERTICAL, 10 FEET FROM ARRAY
1.0 FEET DEEP (AV10, 1.5, 1)
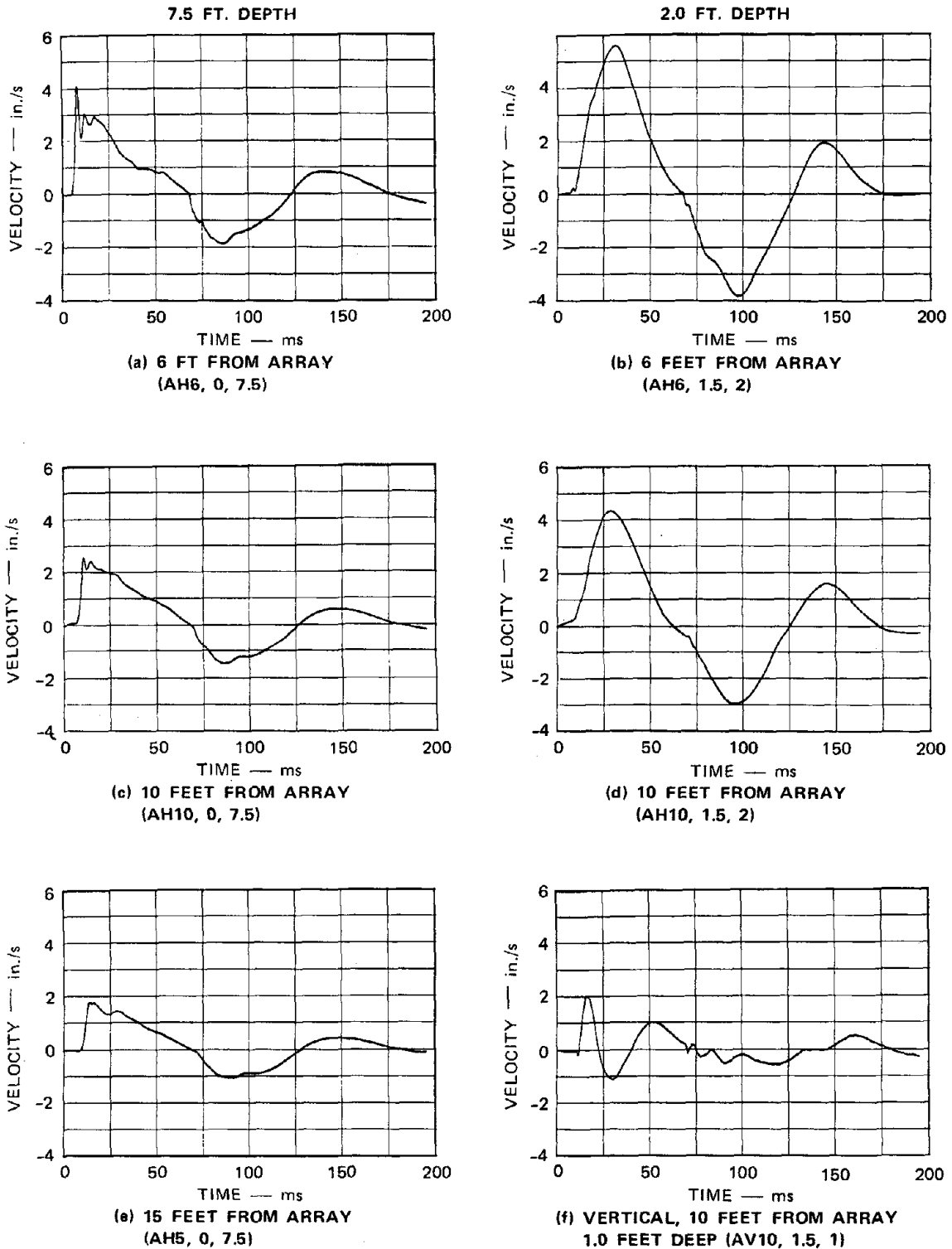
MA-7556-18

FIGURE 20   VARIATION OF VELOCITY WITH DISTANCE AND DEPTH FOR ARRAY TEST, $v = \int a\, dt$

Test 132, 10.6 gm/ft PETN and canister vent area 0.056 in.^{2}/ft per source.

44

Figure 21 shows the displacement-time histories calculated by twice integrating the six accelerometer records given in Figure 19. Again, in contrast to the single-source results (Figure 8), the displacements are significant both at depth and near the surface. Comparison of Figures 21(a), 21(c), and 21(e) shows that with increasing distance from the array the displacement-time histories change in amplitude but not in shape. This decay in amplitude with distance follows that predicted by the quasi-static elliptical theory presented in Appendix A.

A close look at these displacement-time histories shows that they are very similar in shape to the soil stress records. This can be seen from Figure 22, which shows the displacement-time and soil stress-time histories at a 10-ft standoff. Since the soil stress in turn follows the source pressure (Figure 17), we conclude that the displacement-time history in the soil can be controlled by controlling the shape and amplitude of the source pressure pulse.

Figure 23 shows a comparison of earth motion from a single source and from an array for both a 7.5-ft and 2.0-ft depth. It is apparent that use of an array greatly enhances velocity and displacement.

C.   Comparison of Tests with Three Different Vent Areas

As mentioned above, array tests were performed with three different central canister vent areas. Up to this point, we have discussed only the test with the largest of these vent areas (Test 132). The three different vent areas were tested in an effort to control the frequency of the earth motion by controlling the pressure rise in the bladder. Figures 24 and 25 show the key results from these three tests: Test 132; Test 131, with one-fourth the vent area of Test 132; and Test 130, with one-half the vent area of Test 132.

Figure 24 shows the bladder pressure and soil stress for these three array tests. Comparison of Figures 24(a) and 24(c) with 24(e) shows that the initial slope of the bladder pressure decreased at about
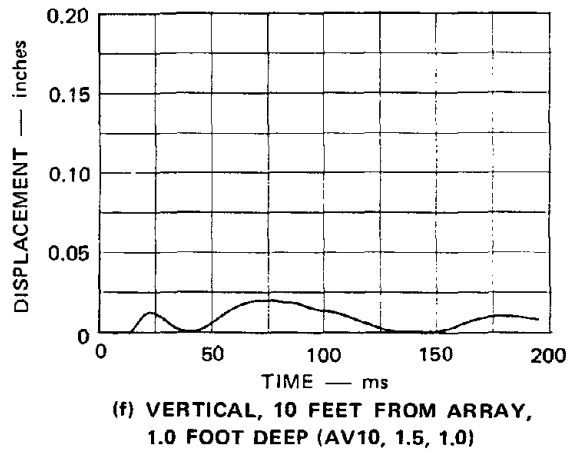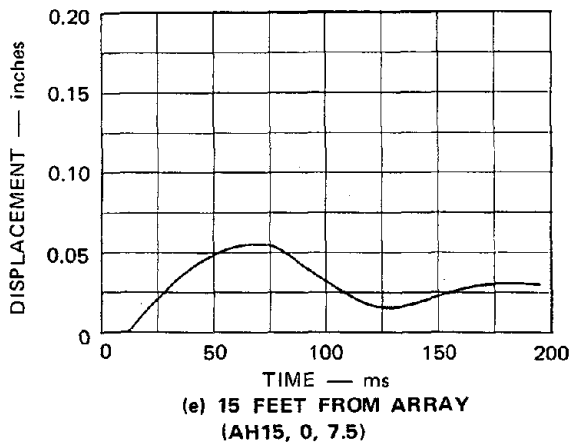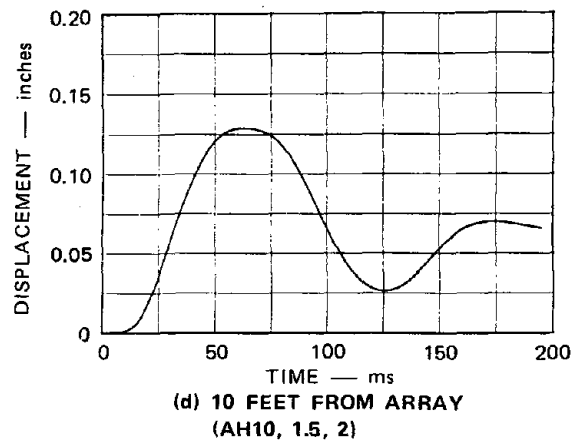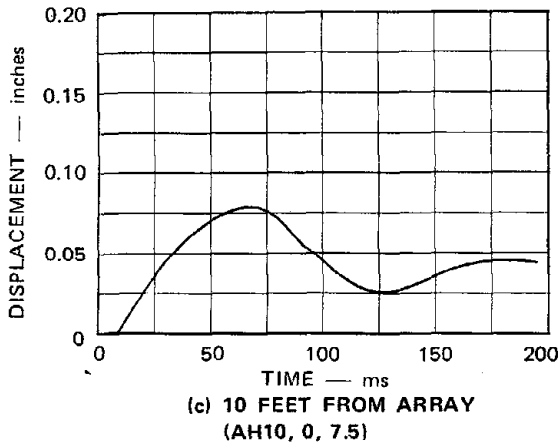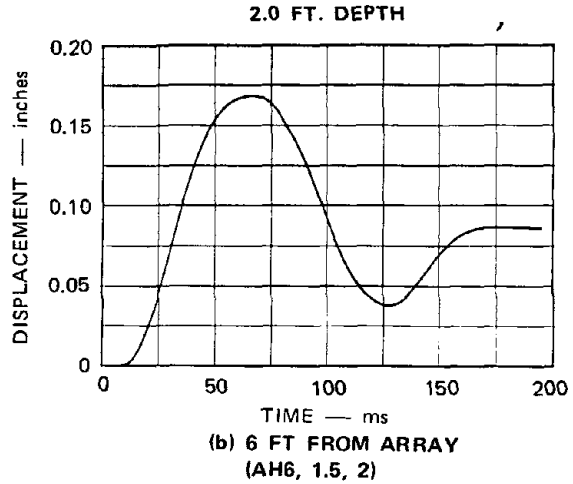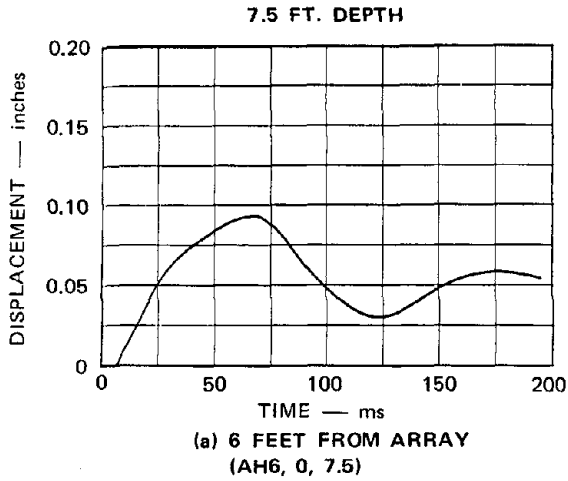
FIGURE 21   VARIATION OF DISPLACEMENT WITH DISTANCE AND DEPTH FOR ARRAY
TESTS, d = ∫ vdt

Test 132, 10.6 gm/ft PETN and canister vent area 0.056 in.^{2}/ft per source.

46
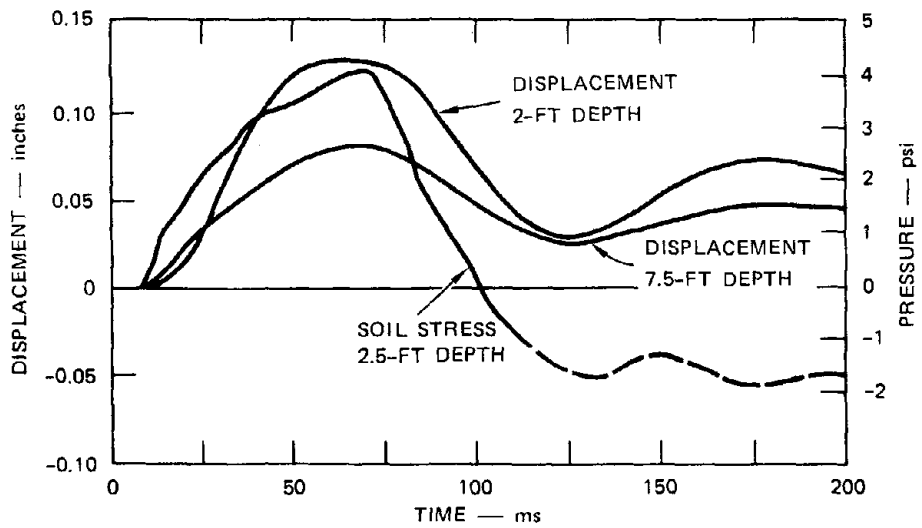
FIGURE 22   COMPARISON OF DISPLACEMENT AND SOIL STRESS,
10 FT FROM ARRAY
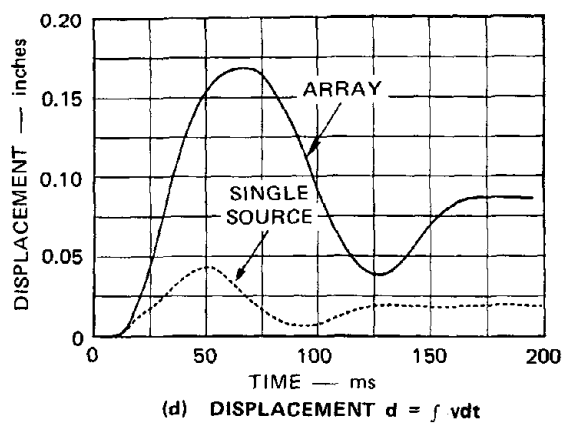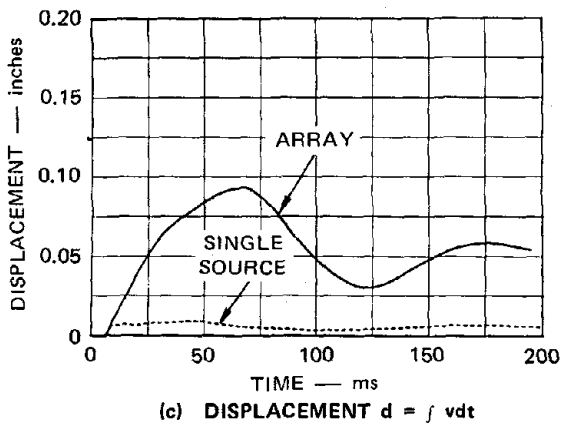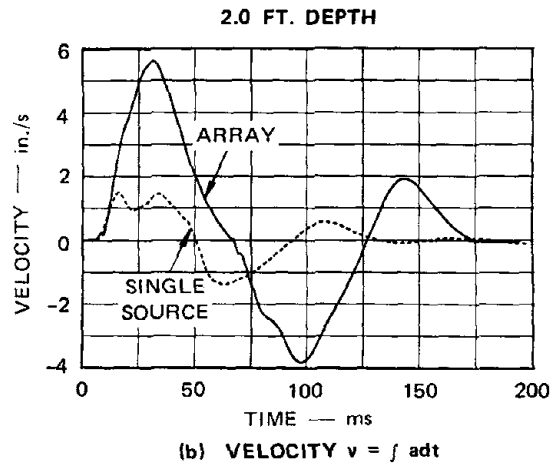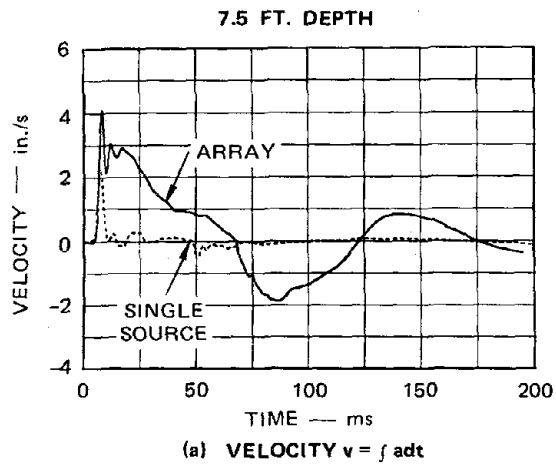
FIGURE 23   COMPARISON OF EARTH MOTION FROM SINGLE-SOURCE AND ARRAY TESTS
(5.5-FT STANDOFF FOR SINGLE SOURCE AND 6.0-FT STANDOFF FOR ARRAY.)
Tests 125 and 132, 10.6 gm/ft PETN and canister vent area 0.055 in.^{2}/ft.

48
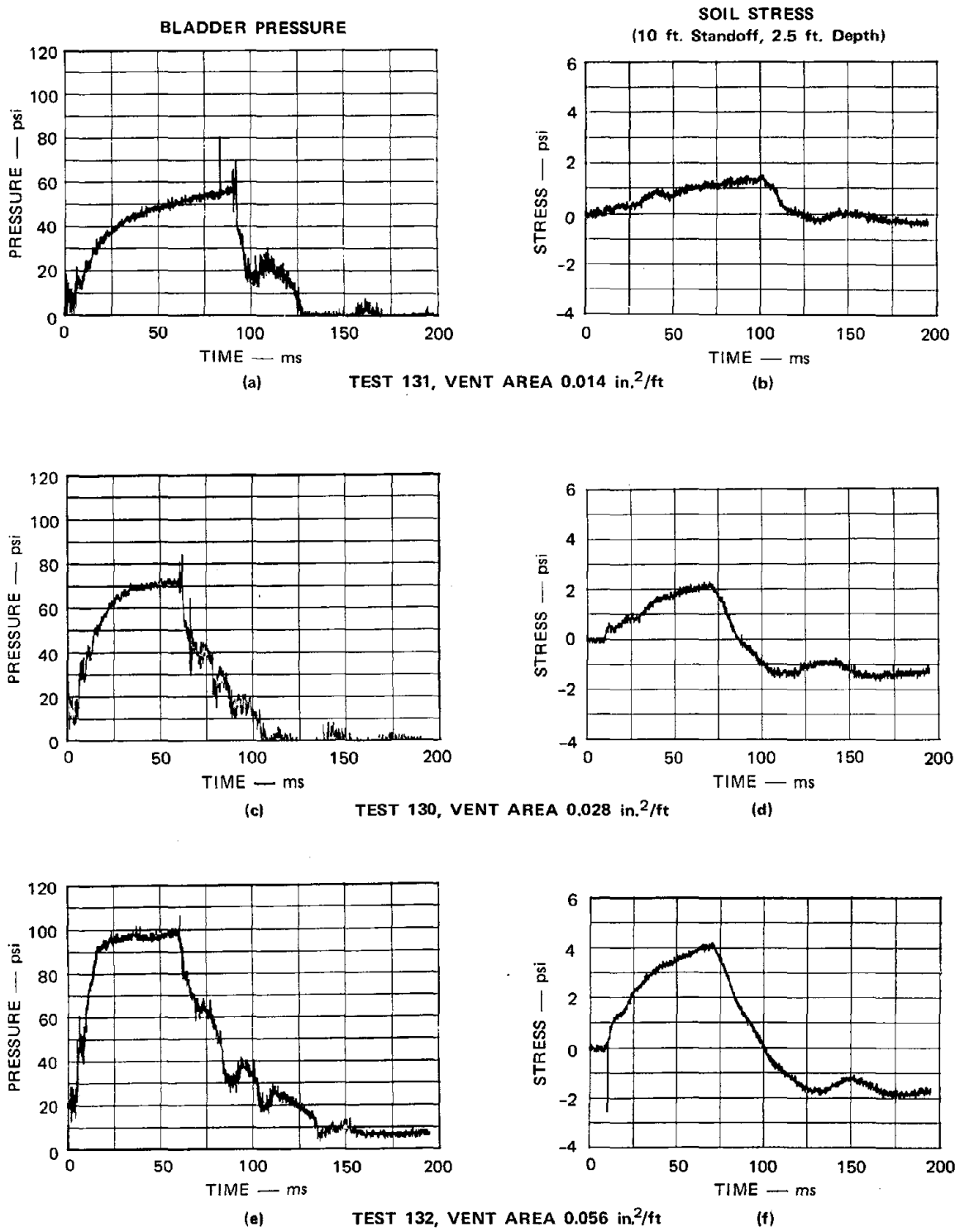
FIGURE 24   VARIATION OF BLADDER PRESSURE AND SOIL STRESS WITH CANISTER VENT
AREA FOR ARRAY TESTS

10.6 gm/ft PETN per source.

49
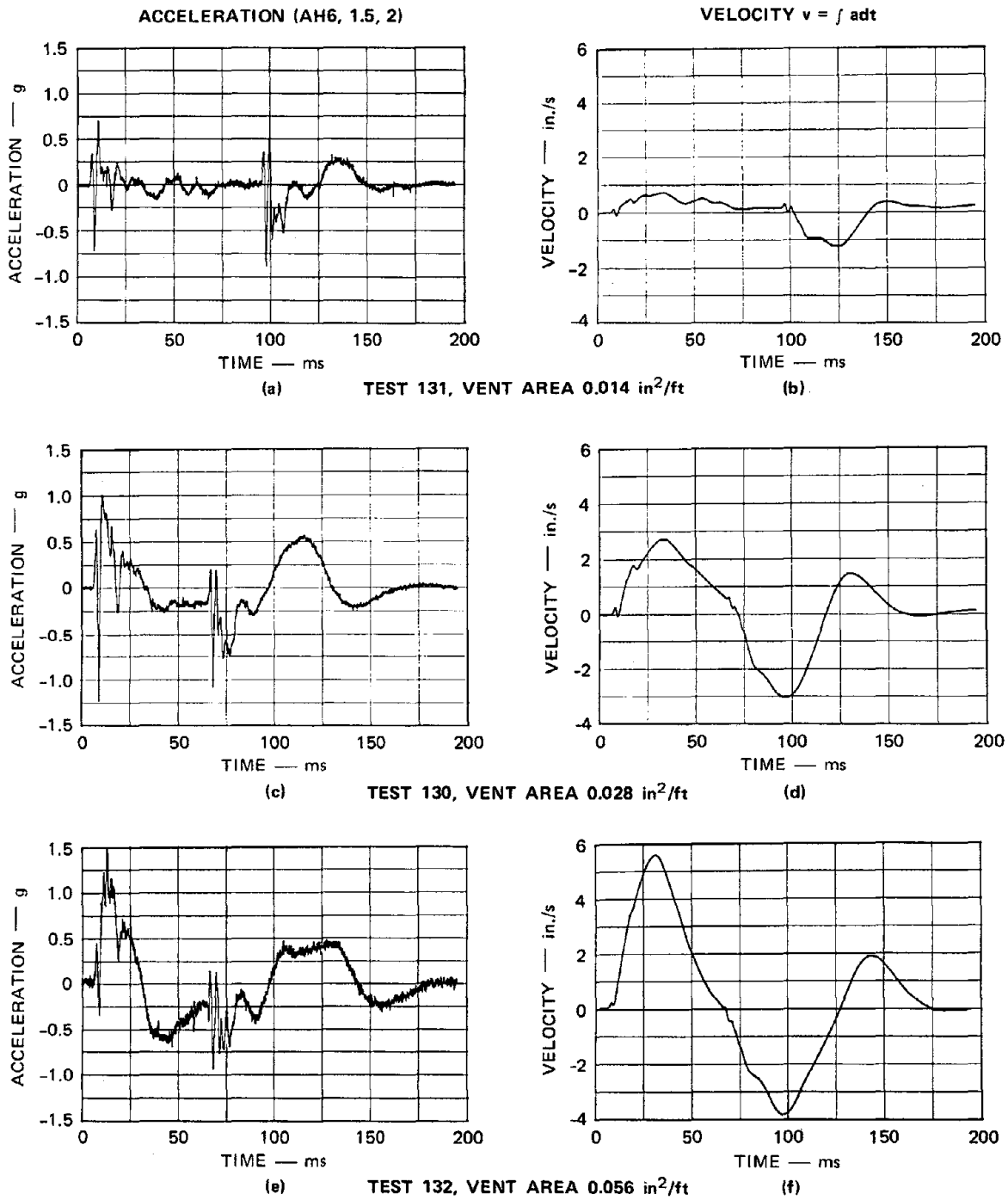
FIGURE 25   VARIATION OF EARTH MOTION WITH CANISTER VENT AREA FOR ARRAY TESTS
10.6 gm/ft per source, 6 ft from source, 2.0 ft deep.

the same rate as the vent area was decreased. The peak bladder pressure was also decreased by decreasing the vent area; this is attributed to heat transfer to the central steel canister. (A rough estimate of energy loss to heat transfer shows that a 50% loss can occur in 60 ms.) This drop in bladder pressure along with the nonlinearity of soil response accounts for the fourfold decrease in soil stress between Figure 24(f) and 24(b).

Figure 25 shows the acceleration- and velocity-time histories for the three array tests. Comparison of the three tests shows that decreasing the canister vent area resulted in a decrease in the amplitude of the ground motion while having little effect on the frequency during the loading pulse (decreased by expansion of bladder). This decrease in amplitude is as expected after examining the decrease in soil stress (Figure 24).

A different phenomena is observed during the exhaust of the explosive products from the bladder (the unloading pulse); there is a decrease in pulse period as the canister vent area is decreased (although the exhaust vent area remains the same). A reason for this can be seen by comparing the bladder pressure records for the three array tests (Figure 24); a decrease in canister vent area results in a decrease in bladder pressure and thus a decrease in the unloading period directly affecting the pulse period.

Figure 26 shows a direct comparison of soil stress- and the displacement-time histories 10 ft from the array for the three different vent areas. It can be seen that soil stress and ground displacement have a similar period and shape, indicating that by proper tailoring of the input pressure at high enough levels, both the period and shape can be controlled.
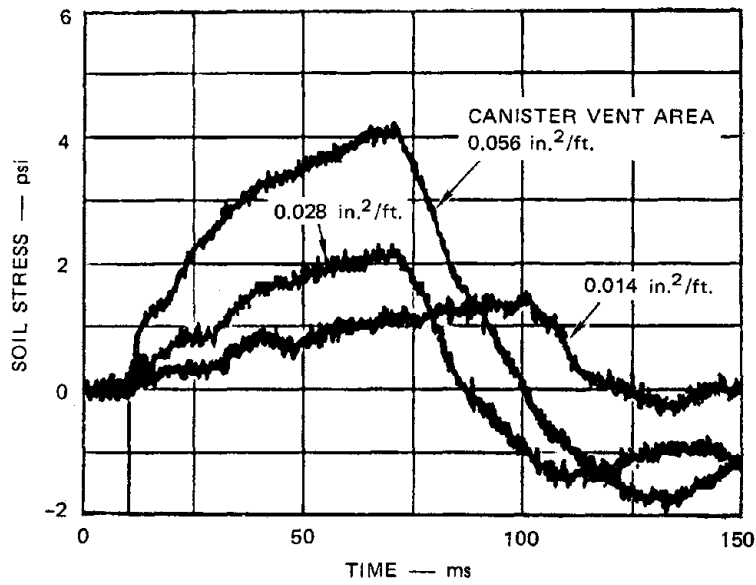
(a) SOIL STRESS — 2.5 FT. DEPTH
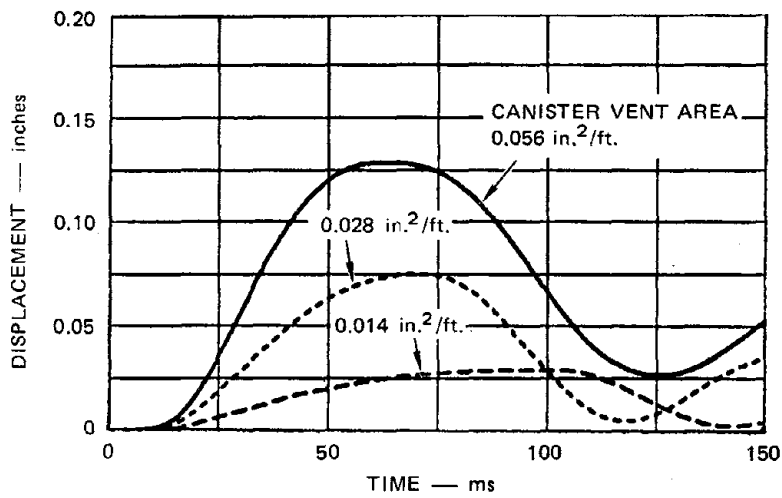
(b) DISPLACEMENT — 2 FT. DEPTH

MA-7556-25

FIGURE 26   SOIL STRESS- AND DISPLACEMENT-TIME HISTORIES
10 FT FROM ARRAY FOR THREE DIFFERENT
VENT AREAS

52

VI CONCLUSIONS AND FUTURE WORK

The results of the past two years' work demonstrate that the con-
tained explosive line source array is a feasible technique for testing
in-situ structures at strong earthquake levels. Tests at 1/3 scale
demonstrate that reasonable amplitudes and frequencies can be coupled
into the earth with a minimum of explosive and with no surface eruptions.
Theoretical extrapolation to a 100 ft wide by 35 ft deep array shows that
150 pounds of explosive will give a peak velocity of about 15 in./sec,
a peak displacement of about 1.5 inches, and a fundamental frequency of
3 Hz. The tests also show that repeatable results can be obtained with
reuse of the same line sources.

Design and testing is now under way to demonstrate that multiple
detonations can be fired within a single source and to simplify con-
struction and improve the performance of the sources. Early this fall,
a larger scale single source will be designed and tested.

Under a new two-year program proposed to begin in early 1980, we
plan to build and test the larger scale, 100 x 35 ft array, consisting of
10 to 12 sources with each source having a 3-pulse-per-test capability.
During the first year the array will be built and tested in the single-
pulse mode. In the second year the 3-pulse-per-test capability will be
added. A 30 x 30 ft test area will be available for structural testing
by SRI and by other researchers as time and space allow.

These tests will provide the technological basis for the long-
range objective of designing groups of arrays, of this size and larger
as needed, that can simulate motions lasting 5 to 10 seconds. For
example, a group of three arrays of the size described above, with each
array adjusted to produce a different pulse duration, could provide a
sequence of eighteen acceleration pulses (nine detonations) and hence a
simulated motion lasting 5 seconds and having a frequency content

53

ranging from 2 to 10 Hz. We envision that such arrays would be built after completion of the above program as a cooperative effort among several universities, or by industrial concerns for use in applied research and immediate application to earthquake resistance certification.

Appendix A

STRESS, STRAIN, AND DISPLACEMENT AROUND A PRESSURIZED ELLIPTICAL HOLE

Analytical Solution

To estimate elastic response around the array, consider the static plane strain problem of a pressurized elliptical hole with major radius $\underline{a}$ and minor radius $\underline{b}$ as shown in Figure A-1. The ellipse is defined in the z plane by

$$\frac{x^2}{a^2} + \frac{y^2}{b^2} = 1 \tag{A-1}$$

The ellipse and the region around it is mapped from a circle and the region within it by the function

$$z = R(\frac{1}{\zeta} + m\zeta), \quad R > 0, \quad |\zeta| \leq 1 \tag{A-2}$$

where

$$z = x + iy = re^{i\theta}, \quad \zeta = \xi + i\eta = \rho e^{i\gamma} \tag{A-3}$$

$$R = \frac{a + b}{2}, \quad m = \frac{a - b}{a + b} \tag{A-4}$$

As γ ranges from 0 to $-\pi/2$, θ ranges from 0 to $+\pi/2$, as shown in the figure. The stress functions for a pressurized ellipse are[*,†]

$$\Phi_1(\zeta) = - PRm\zeta \tag{A-5}$$

$$\Psi_1(\zeta) = - PR\left[\zeta + \frac{m\zeta(\zeta^2 + m)}{1 - m\zeta^2}\right] \tag{A-6}$$

---

[*] I. S. Sokolnikoff, _Mathematical Theory of Elasticity_ (McGraw-Hill, New York, 1956), pp. 292-295.

[†] Since response is entirely elastic, the pressure P is associated with the elastic pressure P_e discussed in Section IV.
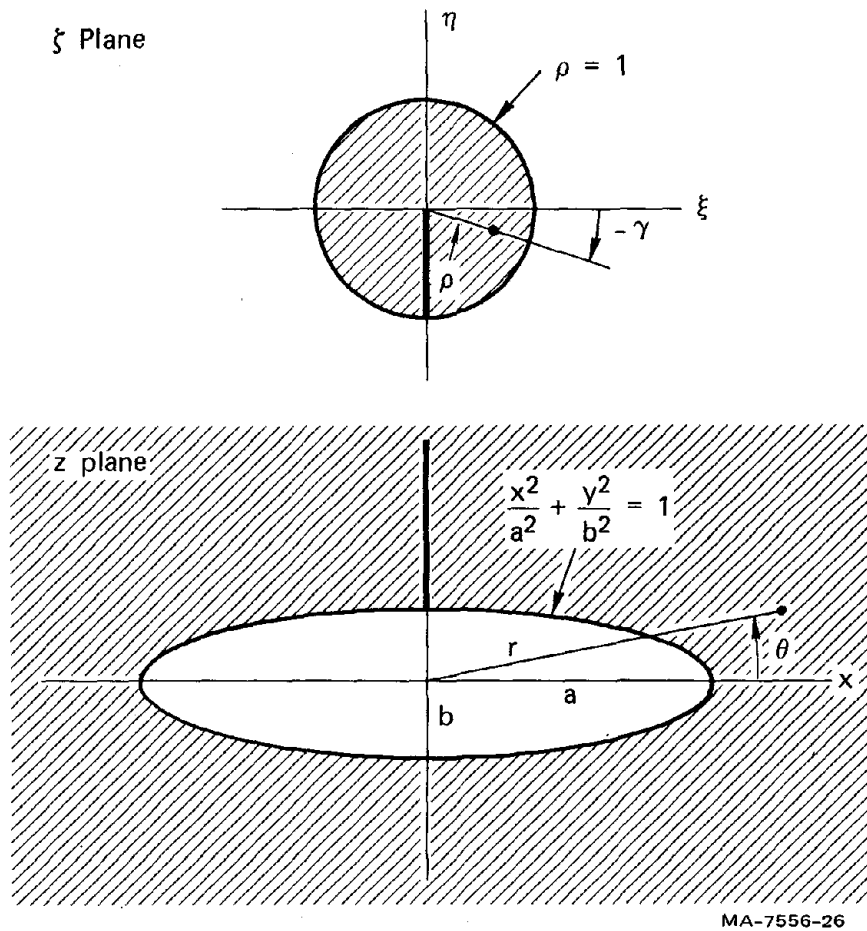
FIGURE A.1   MAPPING OF CIRCULAR AREA ONTO AREA EXTERNAL
             TO AN ELLIPTICAL HOLE

Stresses and displacements are found from the general formulas:

$$\sigma_x + \sigma_y = 4\mathcal{R}[\Phi'(z)] \tag{A-7}$$

$$\sigma_x - \sigma_y + 2i\tau_{xy} = 2[\bar{z}\Phi''(z) + \Psi'(z)] \tag{A-8}$$

$$2\mu(u_x + iu_y) = \kappa\Phi(z) - z\overline{\Phi'(z)} - \overline{\Psi(z)} \tag{A-9}$$

where

$$2\mu = \frac{E}{1+\nu}, \quad \kappa = 3 - 4\nu \text{ (plane strain)} \tag{A-10}$$

and

$$\Phi[z(\zeta)] \equiv \Phi_1(\zeta), \quad \Psi[z(\zeta)] \equiv \Psi_1(\zeta) \tag{A-11}$$

Therefore,

$$\Phi'(z) = \frac{d\Phi_1}{d\zeta}\frac{d\zeta}{dz} = \frac{-\zeta^2}{R(1-m\zeta^2)}\frac{d\Phi_1}{d\zeta} \tag{A-12}$$

and so forth.

Substitution of the stress functions in Eqs. (A-5) and (A-6) into Eqs. (A-7) and (A-8) gives the desired expressions for stresses:

$$\sigma_y + \sigma_x = \frac{4P}{D}(f\cos 2\gamma - f^2) \tag{A-13}$$

$$\sigma_y - \sigma_x = \frac{2P}{D^3}\left\{-3Mf^2(1-f^2) + [Mf(1-f^4) + 4f^2(1-f^2)]\cos 2\gamma \right.$$
$$\left. +[Mf^2(1-f^2) - 2f(1-f^4)]\cos 4\gamma\right\} \tag{A-14}$$

$$\tau_{xy} = \frac{P}{D^3}\left\{[MF(1-6f^2+f^4) + 4f^2(1+f^2)]\sin 2\gamma \right.$$
$$\left. +[Mf^2(1+f^2) - 2f(1+f^4)]\sin 4\gamma\right\} \tag{A-15}$$

in which

$$D = 1 - 2f \cos 2\gamma + f^2, \qquad f = m\rho^2, \qquad M = \frac{1 + m^2}{m} \qquad (A-16)$$

Displacements are similarly found, by using Eqn. (A-9):

$$u_y = \frac{PR}{2\mu} \left\{ - [(1 + 2m)\rho + mQ(1 + \rho^2 + m\rho^2)] \sin \gamma + Q \sin 3\gamma \right\} \qquad (A-17)$$

$$u_x = \frac{PR}{2\mu} \left\{ [(1 - 2m)\rho + mQ(1 + \rho^2 - m\rho^2)] \cos \gamma - Q \cos 3\gamma \right\} \qquad (A-18)$$

in which

$$Q = m\rho(1 - \rho^2)/D \qquad (A-19)$$

Numerical Results

It is convenient to calculate these quantities along ρ, γ contours. These map onto ellipses (ρ = constant) and hyperbolas (γ = constant) in the z plane, given in parametric form by expanding Eq. (A-1) as follows:

$$\frac{x}{R} = (m\rho + \frac{1}{\rho}) \cos \gamma, \qquad \frac{y}{R} = (m\rho - \frac{1}{\rho}) \sin \gamma \qquad (A-20)$$

Tabulations of z-contours, displacements, and stresses for m = 0.8 are given in Tables A-1, A-2, and A-3. The displacement data are plotted in the z-plane in Figure A-2. Also shown in Figure A-2 are the locations of the accelerometers in the array tests reported in the main text. These are plotted by taking the end of the ellipse, x/R = 1.8, to coincide with the 15-foot half-length of the array. Corresponding dimensions in feet are given as a second set of coordinates in the figure.

Displacement in the y direction is plotted in Figure A-3 as a function of distance y from the array for several contours γ = const. A structure to be tested would be placed at about y/R = 0.8 (about 7 feet for the 30-foot array). Contours corresponding to a 10 x 10 foot structure placed with its closest side at this range are drawn in Figures A-2 and A-3. The centerline of the structure lies on the $\gamma = 0°$ curve, as shown in both figures. Either side of the structure is on the dashed contour in Figure A-3. The front and rear of the structure are the lines at y = 7 and 17 feet. The closeness of centerline and side contours in Figure A-3 shows

A-4

Table A-1 ELLIPSE/HYPERBOLA CONTOURS FOR m = 0.8

γ \ ρ		1	0.9	0.8	0.7	0.6	0.5	0.4	0.3	0.2
0°	x/R	1.80	1.83	1.89	1.99	2.15	2.40	2.82	3.57	5.16
	y/R	0	0	0	0	0	0	0	0	0
-15°	x/R	1.74	1.77	1.83	1.92	2.07	2.32	2.72	3.45	4.98
	y/R	0.05	0.10	0.16	0.22	0.31	0.41	0.56	0.80	1.25
-30°	x/R	1.56	1.59	1.64	1.72	1.86	2.08	2.44	3.09	4.47
	y/R	0.10	0.20	0.31	0.43	0.59	0.80	1.09	1.55	2.42
-45°	x/R	1.27	1.29	1.34	1.41	1.52	1.70	1.99	2.53	3.65
	y/R	0.14	0.28	0.43	0.61	0.84	1.13	1.54	2.19	3.42
-60°	x/R	0.90	0.92	0.95	0.99	1.07	1.20	1.41	1.79	2.58
	y/R	0.17	0.30	0.53	0.75	1.03	1.39	1.89	2.68	4.19
-75°	x/R	0.47	0.47	0.49	0.51	0.56	0.62	0.73	0.92	1.34
	y/R	0.19	0.38	0.59	0.84	1.15	1.55	2.11	2.99	4.68
-90°	x/R	0	0	0	0	0	0	0	0	0
	y/R	0.20	0.39	0.61	0.87	1.19	1.60	2.18	3.09	4.84

Table A-2   DISPLACEMENTS AROUND PRESSURIZED ELLIPSE FOR m = 0.8
(Normalized to PR/2μ)

γ \ ρ		1	0.9	0.8	0.7	0.6	0.5	0.4	0.3	0.2
0°	u_x	−0.60	−0.62	−0.57	−0.51	−0.45	−0.38	−0.30	−0.23	−0.15
	u_y	0	0	0	0	0	0	0	0	0
−15°	u_x	−0.58	−0.43	−0.36	−0.32	−0.28	−0.24	−0.20	−0.15	−0.10
	u_y	0.67	0.51	0.38	0.28	0.21	0.16	0.12	0.09	0.06
−30°	u_x	−0.52	−0.32	−0.18	−0.08	−0.02	0.00	0.01	0.01	0.01
	u_y	1.30	1.17	1.00	0.82	0.65	0.50	0.37	0.26	0.17
−45°	u_x	−0.42	−0.25	−0.09	0.03	0.12	0.16	0.17	0.15	0.11
	u_y	1.84	1.72	1.56	1.38	1.17	0.95	0.74	0.54	0.35
−60°	u_x	−0.30	−0.17	−0.05	0.06	0.14	0.19	0.21	0.20	0.15
	u_y	2.25	2.14	1.99	1.82	1.61	1.37	1.11	0.84	0.56
−75°	u_x	−0.16	−0.09	−0.02	0.04	0.09	0.12	0.14	0.13	0.10
	u_y	2.51	2.40	2.26	2.08	1.89	1.65	1.37	1.06	0.73
−90°	u_x	0	0	0	0	0	0	0	0	0
	u_y	2.60	2.49	2.35	2.19	1.99	1.75	1.47	1.15	0.79

Table A-3 STRESSES AROUND PRESSURIZED ELLIPSE FOR m = 0.8
(Normalized by internal pressure P; tension is positive)

γ \\ ρ		1	0.9	0.8	0.7	0.6	0.5	0.4	0.3	0.2
0°	σ_x	−1.00	2.46	1.77	1.17	0.76	0.48	0.28	0.15	0.06
	σ_y	17.00	4.91	2.43	1.41	0.86	0.52	0.30	0.16	0.07
	τ_{xy}	0	0	0	0	0	0	0	0	0
−15°	σ_x	1.42	0.60	0.05	0.03	0.09	0.11	0.09	0.06	0.03
	σ_y	−0.58	1.30	1.88	1.54	1.05	0.66	0.38	0.20	0.08
	τ_{xy}	−1.00	−1.47	−0.70	−0.14	+0.06	0.10	0.08	0.05	0.02
−30°	σ_x	−0.17	0.14	0.07	−0.12	−0.22	−0.20	−0.14	−0.08	−0.03
	σ_y	−0.97	−0.64	−0.10	+0.34	0.52	0.49	0.36	0.21	0.10
	τ_{xy}	−0.16	−0.56	−0.78	−0.69	−0.46	−0.24	−0.10	−0.03	−0.01
−45°	σ_x	−0.57	−0.27	−0.10	−0.07	−0.11	−0.15	−0.15	−0.11	−0.06
	σ_y	−0.99	−0.92	−0.73	−0.46	−0.19	−0.00	+0.09	0.09	0.05
	τ_{xy}	−0.05	−0.21	−0.40	−0.52	−0.52	−0.43	−0.29	−0.16	−0.07
−60°	σ_x	−0.71	−0.47	−0.26	−0.13	−0.06	−0.04	−0.04	−0.04	−0.02
	σ_y	−1.00	−0.97	−0.90	−0.78	−0.60	−0.41	−0.24	−0.12	−0.04
	τ_{xy}	−0.02	−0.09	−0.19	−0.29	−0.35	−0.36	−0.30	−0.21	−0.10
−75°	σ_x	−0.76	−0.55	−0.36	−0.18	−0.05	0.02	0.05	0.05	0.03
	σ_y	−1.00	−0.99	−0.96	−0.89	−0.79	−0.64	−0.47	−0.29	−0.14
	τ_{xy}	−0.01	−0.03	−0.08	−0.13	−0.17	−0.19	−0.18	−0.14	−0.07
−90°	σ_x	−0.78	−0.58	−0.38	−0.21	−0.06	+0.04	0.09	0.09	0.05
	σ_y	−1.00	−0.99	−0.97	−0.92	−0.84	−0.71	−0.54	−0.35	−0.18
	τ_{xy}	0	0	0	0	0	0	0	0	0
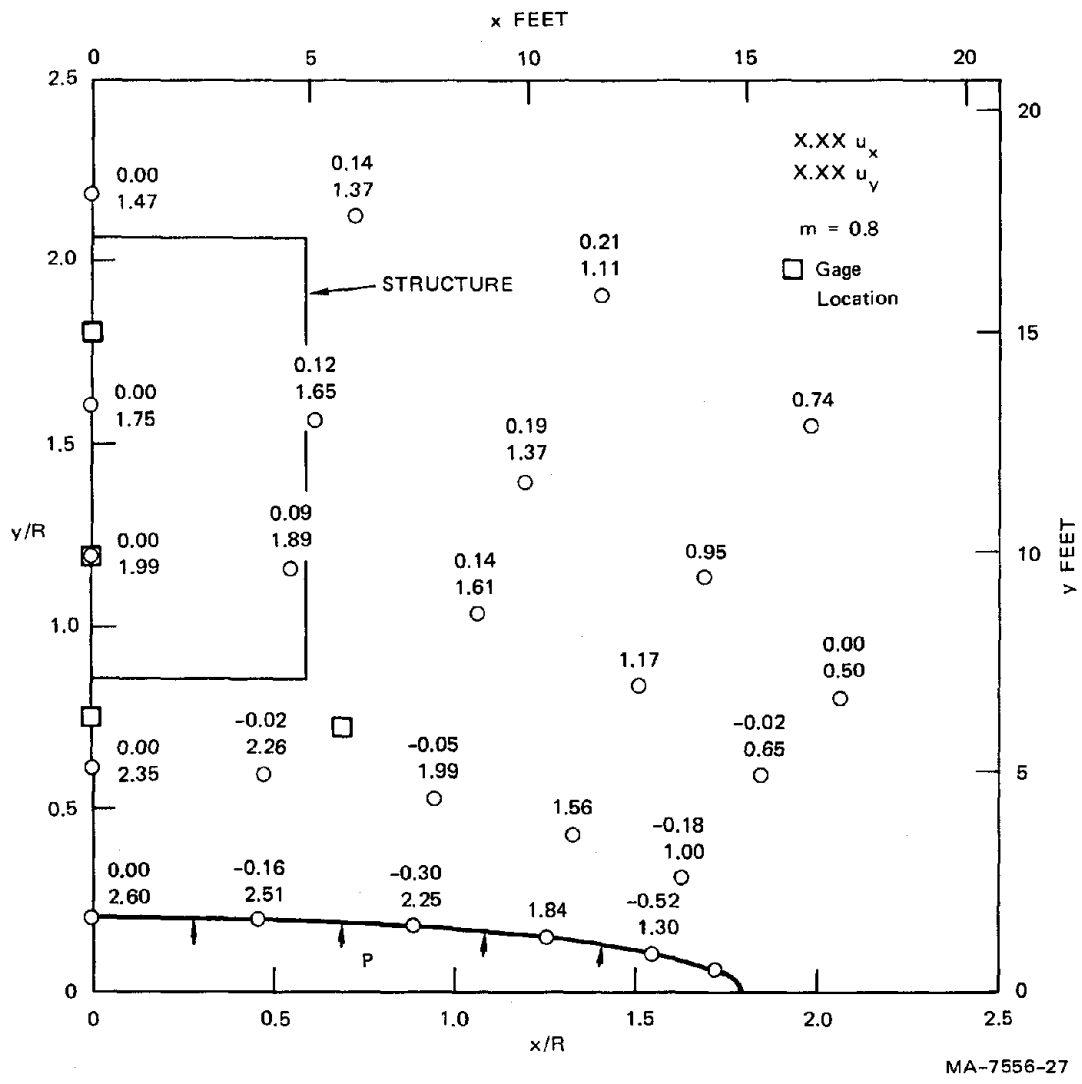
FIGURE A.2   DISPLACEMENTS AROUND PRESSURIZED ELLIPSE
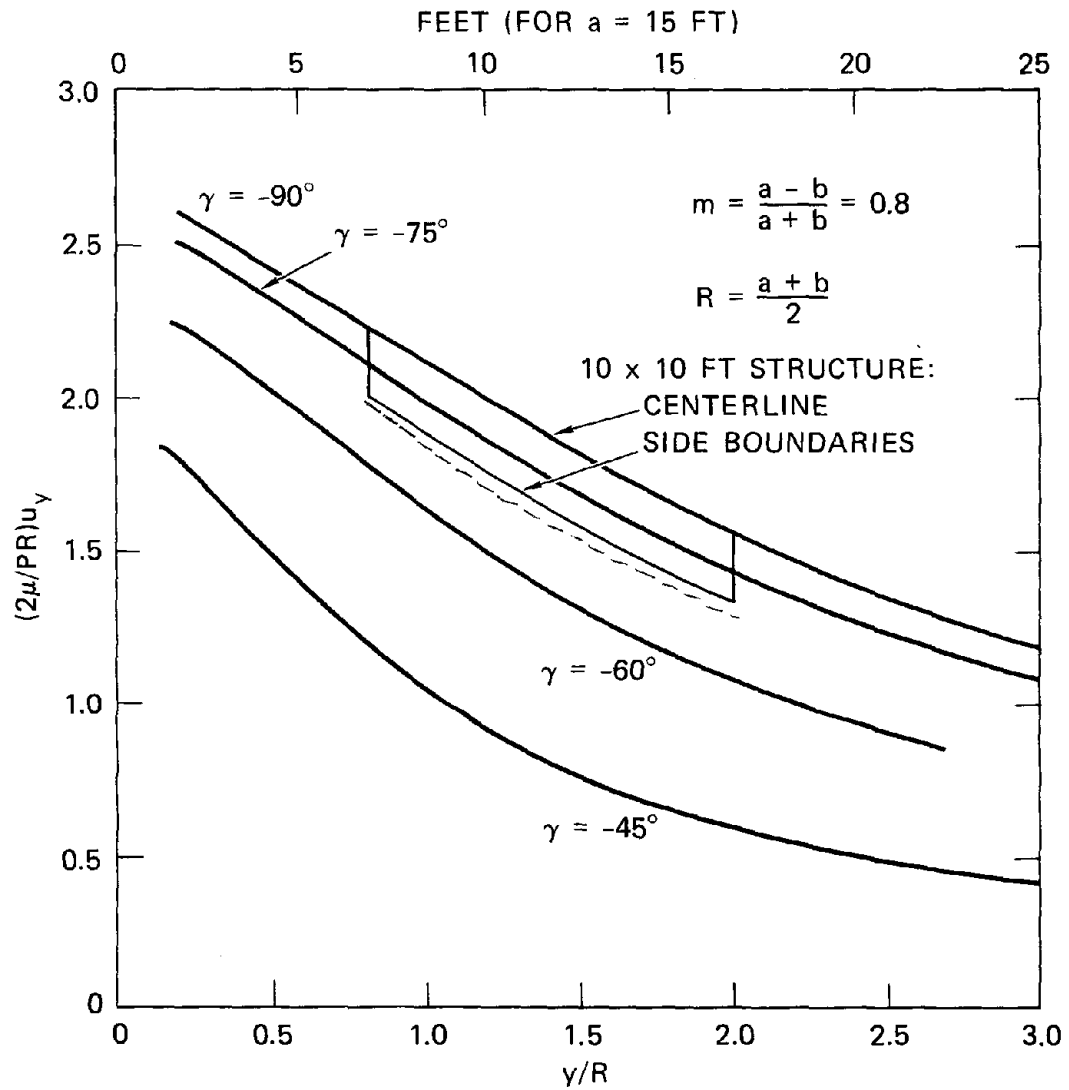(NORMALIZED TO PR/2μ)

FEET (FOR a = 15 FT)

FIGURE A.3   DISPLACEMENT ALONG y-AXIS VERSUS y

MA-7556-28

that displacements are very nearly uniform across the width of the structure. The largest variation in displacement is from front to rear. On the centerline, the normalized displacement is 2.24 at the front and 1.55 at the rear, a difference of 31% of the larger value. This difference is caused by the soil strain under the action of the loading pressure P; that is, by the strain corresponding to the stresses in Table A-3. This soil strain will induce compressive stress in the structure and perhaps some slipping and certainly shearing in the soil as the soil and structure interact.

This situation is similar to, but not identical with, the soil strain and displacement relation for a P-wave incident on the structure. In both instances, the force that moves the soil is from normal stress. By contrast, for an S-wave induced by base rock motion, displacements are constant in horizontal planes so there is no variation across the structure. In this instance the force that moves the soil is from shear stress, so that for any finite imbedment depth of the structure, stresses and perhaps slipping will result because of the strain change between the soil free-field and the structure. All these soil-structure interactions are a subject of great concern for earthquake engineering of structures.

The difference between the soil strain for the array simulation and for a P-wave is in the time phasing between displacement and strain. If motion in both consisted entirely of free wave motion, the phasing would be the same for both. The difference in phasing is a maximum when the simulation motion is produced by a quasi-static stress system (i.e., when the array dimension is small compared with the wavelength of motion frequency, as assumed for simplicity in this appendix). In this case, the displacement and strain are in phase in the simulation because all quantities increase and decrease together in a quasi-static manner. For a P-wave, the displacement u_y and strain ε_y are not in phase because stress, and hence strain, is equal to the wave impedance ρc (density times wave velocity) times the particle velocity $\dot{u}_y$. Thus, for a steady sinusoidal wave train, the strain and particle velocity lag 90° behind the displacement.

For many frequencies of interest, the magnitude of the soil strain in the array simulation is in the same range as that in a P-wave train. In the extreme case of quasi-static motion, the displacement and strain can be related by the pressurized ellipse calculation. Near the ellipse on the minor axis, where a structure would be placed, the displacement, from Eq. (A-17) with $\gamma = -90°$ and $\rho = 1$, is

$$u_y = (1 + 2m) \frac{PR}{2\mu} = 2.6 \frac{PR(1 + \nu)}{2E} \tag{A-21}$$

The strain, from Hooke's law in plane strain and the stresses in Table A-3, is

$$\varepsilon_y = \frac{1}{E}[(1 - \nu^2)\sigma_y - \nu(1 + \nu)\sigma_x]$$

$$= \frac{1}{E}[(1 - \nu^2)P - \nu(1 + \nu)(0.78P)] \tag{A-22}$$

with compressive strain now taken positive. The ratio is

$$\frac{\varepsilon_y}{u_y} = \frac{(1 - \nu^2) - \nu (1 + \nu)(0.78)}{1.3(1 + \nu)R} = \frac{1 - 1.78}{1.3R}$$

$$= 0.43/R \approx 1.71/L \tag{A-23}$$

in which we have taken $\nu = 1/4$ and $R = (a + b)/2 \approx a/2 = L/4$. For the array tests described in the main text, the array length is $L = 30$ feet so that the soil strain is $\varepsilon_y/u_y = 1.17/30$ feet $= 0.057$ per foot of displacement.

For a P-wave train of frequency $\omega = 2\pi f$ (again neglecting the free surface, as in the ellipse solution) the displacement is

$$u_y = U \sin \omega \left(\frac{y}{c} - t\right) \tag{A-24}$$

in which U is the peak displacement and c is the dilational wave velocity.

The strain is

$$\varepsilon_y = \frac{du_y}{dy} = \frac{\omega}{c} \cdot U \cos \omega \left(\frac{y}{c} - t\right) \qquad \text{(A-25)}$$

This demonstrates the previous statement that the strain lags the displacement by 90°. The ratio of peak strain to peak displacement is

$$\frac{|\varepsilon_y|}{|u_y|} = \frac{\omega}{c} \qquad \text{(A-26)}$$

In the experiments, the observed wave speed was c = 1000 fps. For the dominant frequency of 8.7 Hz in the experiments, a P-wave strain-to-displacement ratio would therefore be

$$\frac{|\varepsilon_y|}{|u_y|} = \frac{2\pi(8.7 \text{ Hz})}{1000 \text{ fps}} = 0.055 \text{ per foot} \qquad \text{(A-27)}$$

This is close to the 0.057 per foot ratio for the ellipse calculation.

These ratios would differ for other frequencies, of course, but at the 30-foot array size, 8.7 Hz is near the central frequencies of interest for a 1/3-scale test. For larger scale experiments the central frequency would be lower and the array length would be longer by the same amount. Eqs. (A-23) and (A-26) therefore show that the strain-to-displacement ratios for both the array and a P-wave would be reduced by the same amount. We conclude that the ratios from the array simulation and from P-waves will always be reasonably close in amplitude—the main difference is in phase. As the frequency is increased, the loading ellipse becomes large compared with the wavelength and the simulation motion approaches that of a P-wave in both phase and amplitude.

Limitations of the Elastic Ellipse Idealization

The plane strain pressurized ellipse analysis is intended to give a first order interpretation of array response in the limit as the pulse duration becomes long compared with the wave transit time across the

length of the array. The calculation neglects (1) dynamic response, important for higher frequencies, (2) the presence of the soil free surface, (3) the finite depth of the array, and (4) inelastic soil response. More complete theoretical analyses that treat all of these shortcomings, both individually and in appropriate groups as theoretical complexity is increased, are being performed with a finite element elastic-plastic code.

An indication of the need to include inelastic response is seen by inspection of the stresses in Table A-3. In the region of high stress concentration near the ends of the ellipse (small γ, ρ near unity), the stresses are several times larger than the internal pressure P. These stresses will induce a plastic zone that will change the shape of the elastic-plastic boundary from the ellipse assumed here, and will also introduce shear stresses at the boundary. Nevertheless, we expect that the net motion and stresses in the region in which a structural test model would be placed will be similar to the estimates here because the structure test region is remote from these plastic zones.